Chapter 6

Underwater granular flows

6.1 Introduction

Avalanches, landslides, and debris flows are geophysical hazards, which involve rapid mass movement of granular solids, water, and air as a single phase system. Globally, landslides cause billions of pounds in damage, and thousands of deaths and injuries each year. Hence, it is important to understand the triggering mechanism and the flow evolution. The momentum transfer between the discrete and continuous phases significantly affects the dynamics of the flow as a whole (Topin et al., 2012). Although certain macroscopic models are able to capture simple mechanical behaviours (Peker and Helvacı, 2007), the complex physical mechanisms occurring at the grain scale, such as hydrodynamic instabilities, formation of clusters, collapse, and transport, (Topin et al., 2011) have largely been ignored. In particular, when the solid phase reaches a high volume fraction, the strong heterogeneity arising from the contact forces between the grains, and the hydrodynamic forces, are difficult to integrate into the homogenization process involving global averages.

In order to describe the mechanism of immersed granular flows, it is important to consider both the dynamics of the solid phase and the role of the ambient fluid (Denlinger and Iverson, 2001). The dynamics of the solid phase alone is insufficient to describe the mechanism of granular flow in a fluid. It is important to consider the effect of hydrodynamic forces that reduce the weight of the solids inducing a transition from dense-compacted to dense-suspended flows, and the drag interactions which counteract the movement of the solids (Meruane et al., 2010). Transient regimes characterized by change in the solid fraction, dilation at the onset of flow and development of excess pore pressure, result in altering the balance between the stress carried by the fluid and that carried by the grains, thereby changing the overall behaviour of the flow.

The presence of a fluid phase in a granular medium has profound effects on its mechanical behaviour. In dry granular media the rheology is governed by grain inertia and static stresses sustained by the contact network depending on the shear-rate and confining pressure, respectively (Midi, 2004). As the fluid inertia and viscosity come into play, complications arise as a result of contradictory effects. On one hand, the fluid may delay the onset of granular flow or prevent the dispersion of the grains by developing negative pore pressures (Pailha et al., 2008; Topin et al., 2011). On the other hand, the fluid lubricates the contacts between grains, enhancing in this way the granular flow, and it has a retarding effect at the same time by inducing drag forces on the grains. The objective of the present study is to understand the differences in the mechanism of flow initiation and kinematics between dry and submerged granular flow. In the present study, 2D Lattice-Boltzmann and Discrete Element Method is used to model the fluid-soil interactions in underwater granular flows. The choice of a 2D geometry has the advantage of cheaper computational effort than a 3D case, making it feasible to simulate very large systems.

6.2 LBM-DEM Permeability

In a 3D granular assembly, the pore spaces between grains are interconnected, whereas in a 2-D assembly, a non-interconnected pore-fluid space is formed as the grains are in contact with each other. Which means that the pore-fluid enclosed between the grains cannot flow to neighbouring pore-spaces. This results in a unnatural no flow condition in a 2-D case (see figure 6.1). In order to overcome this difficulty, a reduction in radius is assumed only during LBM computations (fluid and fluid – solid interaction). The reduced radius of the soil grain, i.e., the *hydrodynamic radius* ‘r’, allows for interconnected pore space through which the pore-fluid can flow similar to 3D behaviour. The reduction in radius is assumed only during LBM computations, hence this technique has no effect on the grain – grain interactions computed using DEM.

Realistically, the hydrodynamic radius can be varied from $r = 0.7R$ to $0.95R$, where ‘R’ is the grain radius. Different permeability can be obtained, for any given initial packing, by varying the hydrodynamic radius of the grains, without changing the actual granular packing. Hence, the hydrodynamic radius represents the permeability of the granular assembly. In another sense, the hydrodynamic radius can be assumed to represent the irregularities on the granular surface. Reducing the hydrodynamic radius represents wider channel and more flow between the grains.

In order to understand the relation between the hydrodynamic radius and the permeability of the granular assembly, horizontal permeability tests are performed by varying the hydrodynamic radius as 0.7R, 0.75R, 0.8R, 0.85R, 0.9 and 0.95R. The transverse permeability of

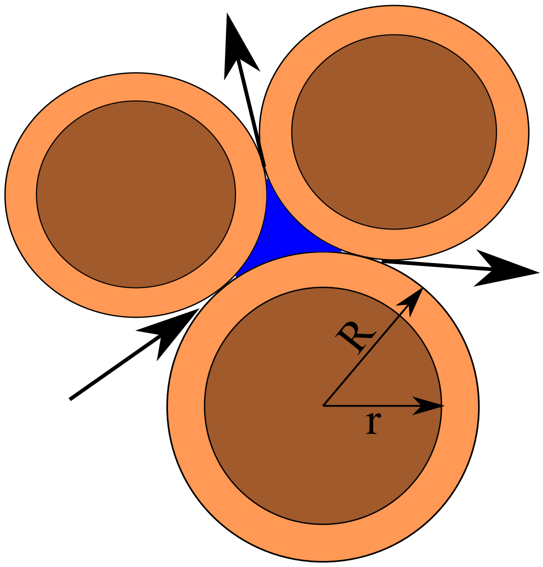

Figure 6.1 Schematic representation of the hydrodynamic radius in LBM-DEM computation

a square sample of 50 mm $\times$ 50 mm filled with poly-disperse ($d_{max}/d_{min} = 1.8$) grains with a mean diameter of 1.7mm is determined. Dirichlet boundary condition (discussed in **??**), i.e., pressure/density constrain is applied along the left and the right boundaries. The density on the left boundary is increased in small increments ($10^{-4}\Delta P$), which a constant density is maintained on the right boundary. This results in a pressure gradient causing the fluid to flow (see figure 6.2).

The mean velocity of flow (v) is determined and the permeability of the sample (k) is computed as:

$$k = v \cdot \mu \cdot \frac{\Delta x}{\Delta P}, \tag{6.1}$$

where μ is the dynamic viscosity of the fluid (Pa s), Δx is the thickness of the bed of porous medium m, and ΔP is the applied pressure difference Pa. For a given hydrodynamic radius, the pressure gradient ΔP is varied to obtain different flow rates. Probing the fluid space showed a Poiseuille flow behaviour between grains. The flow is still within the Darcy's laminar flow regime, which is verified by the linear slope between the pressure gradient and mean flow velocity (see figure 6.3). It can be observed that with increase in the hydrodynamic radius the permeability decreases, i.e., the slope of the mean flow velocity to the pressure gradient decreases. At very low pressure gradient ($\Delta P \leq 0.1$), both 0.9R and 0.95r has a no flow condition. A hydrodynamic radius of $r = 0.95R$ shows almost no flow behaviour, even at higher pressure gradients. A high value of hydrodynamic radius $r > 0.95R$ results in unnatural flow behaviour. Hence, hydrodynamic radii in the range of 0.7 to 0.95R are adopted in the present study.

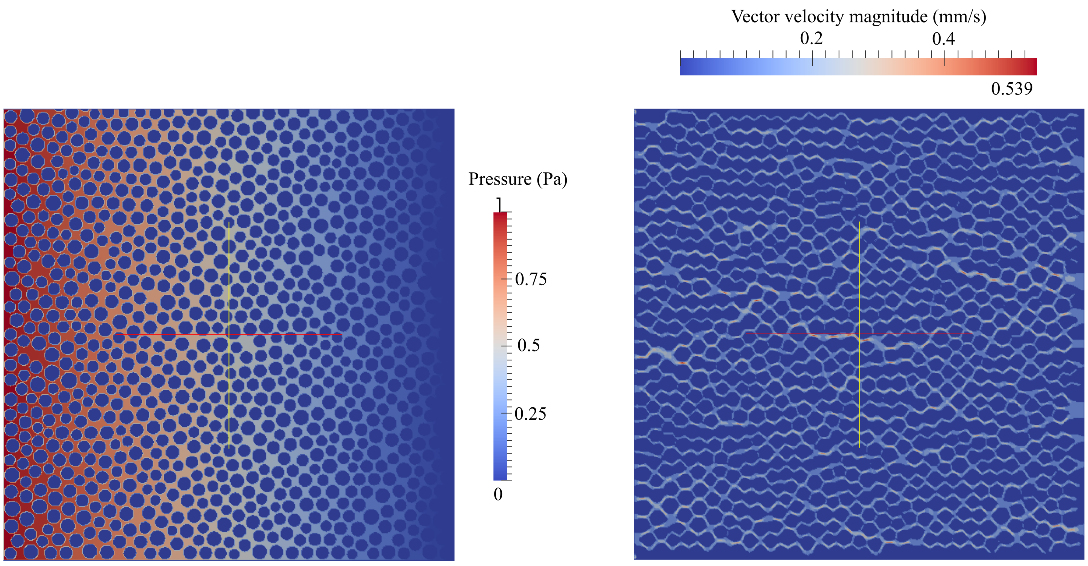

(a) Pressure gradient in the granular assembly (b) Horizontal flow due to pressure gradient

Figure 6.2 Evaluation of the horizontal permeability for a hydrodynamic radius of 0.7R.

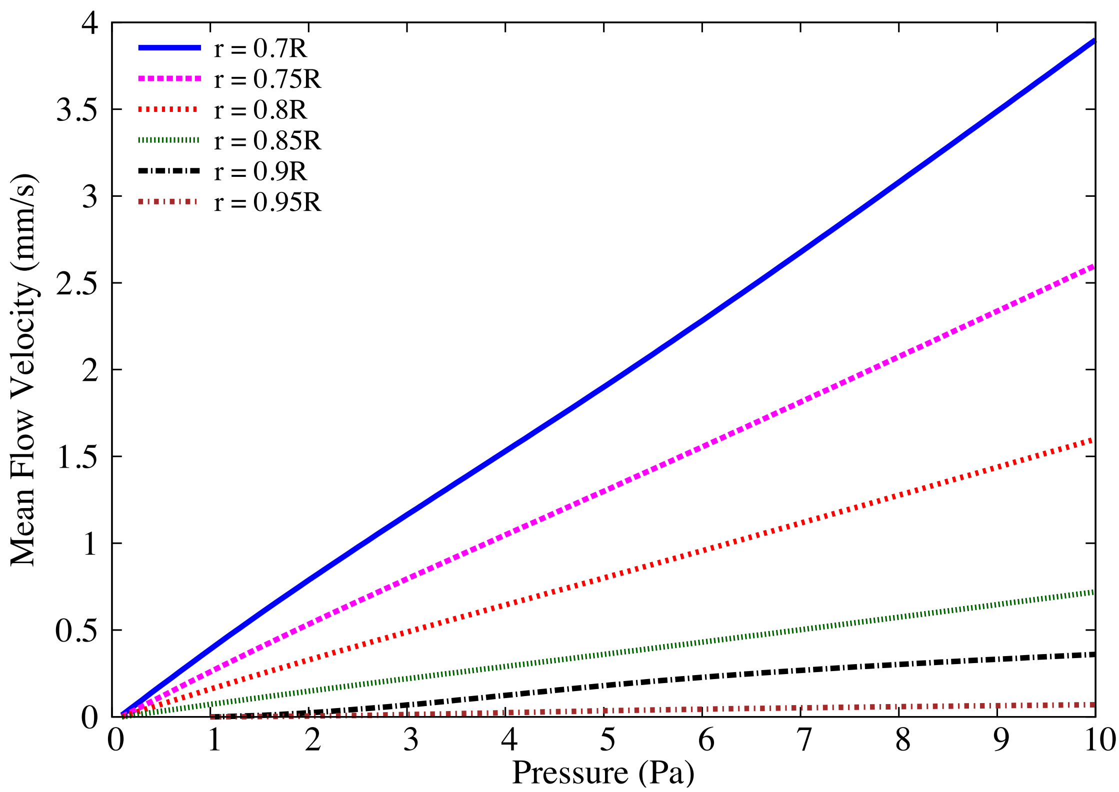

Figure 6.3 Variation of the mean flow velocity with pressure gradient for different hydrodynamic radius.

Increase in the hydrodynamic radius from 0.7 to 0.95 reduces the porosity from 0.60 to 0.27. The permeability computed from LB – DEM method is verified by comparing it with the analytical solution. One of the widely used analytical solution for permeability is the Carman – Kozeny equation (CK Model), which is based on the Poiseuille flow through a pipe and is mainly used for 3D, homogeneous, isotropic, granular porous media at moderate porosities. In the present study, a modified Carman – Kozeny equation that takes into account the micro-structure of the fibres and that is valid in a wide range of porosities is adopted (Yazdchi et al., 2011). The normalized permeability is defined as

$$\frac{k}{d^2} = \frac{\varepsilon}{\psi_{CK}(1-\varepsilon)^2}\,. \tag{6.2}$$

In the CK model, the hydraulic diameter D_h , is expressed as a function of measurable quantities: porosity and specific surface area

$$D_h = \frac{4\varepsilon V}{S_v} = \frac{\varepsilon d}{(1-\varepsilon)}\,, \tag{6.3}$$

$$a_v = \frac{\text{grain surface}}{\text{grain volume}} = \frac{S_v}{(1-\varepsilon V)} = \frac{4}{d}\,, \tag{6.4}$$

where S_v is the total wetted surface, and a_v is the specific surface area. The above value of a_v is for circles (cylinders) - for spheres $a_v = 6/d$. ψ_{CK} is the empirically measured CK factor, which represents both the shape factor and the deviation of flow direction from that in a duct. It is approximated for randomly packed beds of spherical grains. The normalized permeability for different porosity obtained by varying the radius from 0.7 to 0.95 is presented in figure 6.4. The normalized permeability is found to match the qualitative trend of the Carman-Kozeny equations. The LB – DEM permeability curve lies between the permeability curves for spherical and cylindrical grain arrangements implying a better approximation of three-dimensional permeability using a 2D granular assembly with a reduced grain radius during LBM computations. Thus using hydrodynamic radius, realistic fluid - grain interactions can be obtained in a 2D geometry.

6.3 Granular collapse in fluid

The collapse of a granular column, which mimics the collapse of a cliff, has been extensively studied in the case of dry granular material, when the interstitial fluid plays no role (see **??**). The problem of the granular collapse in a liquid,which is of importance for submarine landslides, has to our knowledge attracted less attention (Rondon et al., 2011). Thompson and Hupper

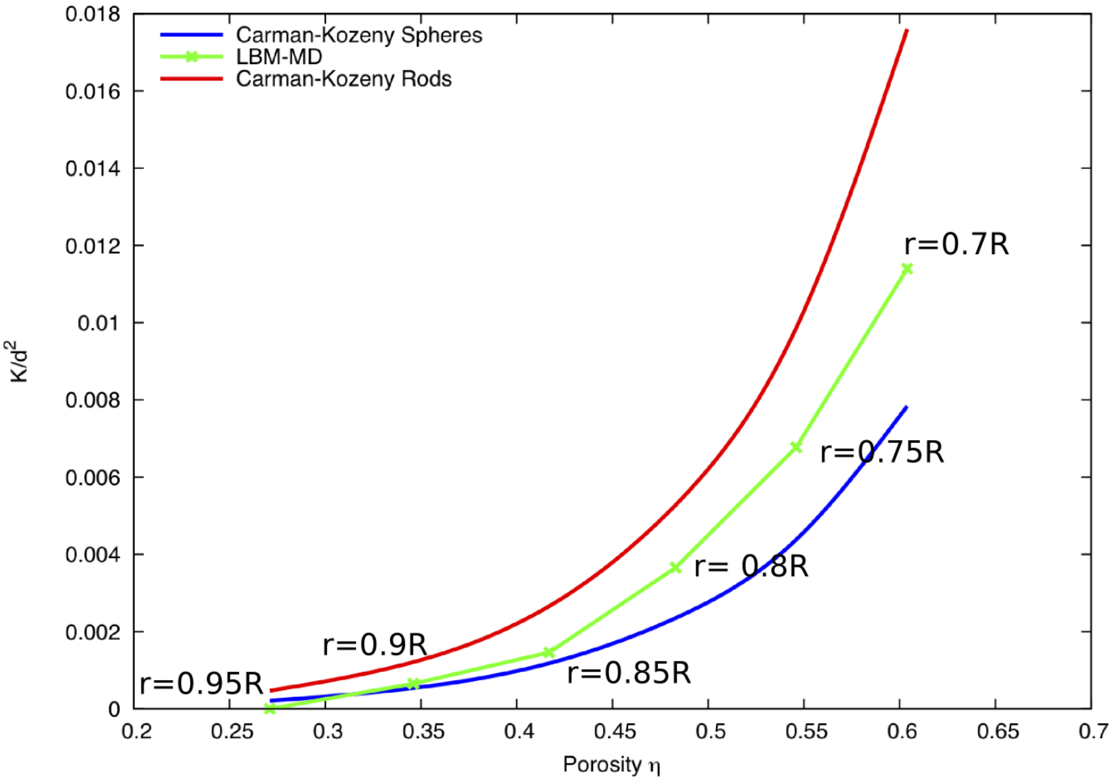

Figure 6.4 Relation between permeability and porosity for different hydrodynamic radius and comparison with the analytical solution.

(2007) observed that the presence of liquid dramatically changes the way a granular column collapses compared to the dry case. The destabilization of a granular pile strongly depends on the initial volume fraction of the packing. For dense packings the granular flow is localized at the free surface of the pile, whereas for loose packings the destabilization occurs in the bulk of the material and has a parabolic profile (Bonnet et al., 2010; Iverson, 2000; Topin et al., 2011).

6.3.1 LBM-DEM set-up

In the present study, the collapse of a granular column in fluid is studied using 2D LBM - DEM. The effect of initial aspect on the run-out behaviour is investigated. The flow kinematics are compared with the dry and buoyant granular collapse to understand the influence of hydrodynamic forces and lubrication on the run-out. Unlike dry column, the role of permeability and the initial volume fraction is expected to have a significant influence on the flow dynamics. Hence the effect of permeability and the initial packing density on the run-out behaviour is investigated.

The granular collapse set-up in fluid is very similar to the dry granular column collapse. A rectangular channel of length L_0 and height H_0 is filled with poly-dispersed discs having $(d_{max}/d_{min} = 1.8)$ (see Figure 6.5). The granular column is then placed in a fluid with a density of $1000\,\mathrm{kg\,m^{-3}}$ and a kinematic viscosity of $1 \times 10^{-6}\,\mathrm{m^2\,s^{-1}}$. The gate supporting the right-hand side boundary of the granular column is opened allowing the column to collapse and flow in fluid. The final run-out distance is measured as L_f and final collapse height as H_f. The collapse takes place on a horizontal surface. The initial aspect ratio of the column is varied as 0.2, 0.4, 0.6, 0.8, 1, 2, 4 and 6.

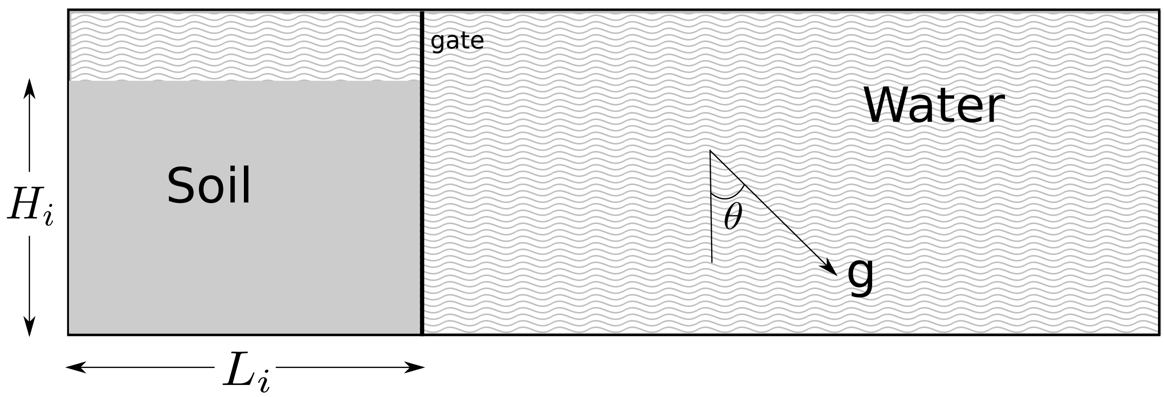

Figure 6.5 Underwater granular collapse set-up.

The cumulative β distribution is adopted to generate grains with d_{max} and d_{min} as 1.25 mm and 2.2 mm, respectively. The soil column is modelled using $\approx$ 2000 discs of density $2650\,\mathrm{kg\,m^{-3}}$ and a contact friction angle of 26°. A linear-elastic contact model is used in the DEM simulations. The granular assemble has a packing fraction of 83%. The critical time step for DEM is computed based on the local contact natural frequency and damping ratio. A sub-cycling time integration is adopted in DEM (see ??). A fluid flow (LBM) time step, $\Delta t = 2.0E^{-}5s$ is determined based on the viscosity and relaxation parameter $\tau = 0.506$. An integer ratio n_s, between the fluid flow time step Δt and DEM time step Δt_D is determined as 15, i.e., every LBM iteration involves a sub-cycle of 15 DEM iterations.

In order to capture realistic physical behaviour of the fluid – grain system, it is essential to model the boundary condition between the fluid and the grain as a non-slip boundary condition, i.e. the fluid near the grain should have similar velocity as the grain boundary. The solid grains inside the fluid are represented by lattice nodes. The discrete nature of lattice, results in a stepwise representation of the surfaces (see figure 6.6), which are otherwise circular, hence sufficiently small lattice spacing h is required. The smallest DEM grain in the system controls the size of the lattice. In the present study, a very fine discretisation of $d_{min}/h = 10$ is adopted, i.e., the smallest grain with a diameter d_min in the system is discretised into 100 lattice nodes $(10h \times 10h)$. This provides a very accurate representation of the interaction between the solid and the fluid nodes. A hydrodynamic radius of 0.7R is adopted during LBM computations.

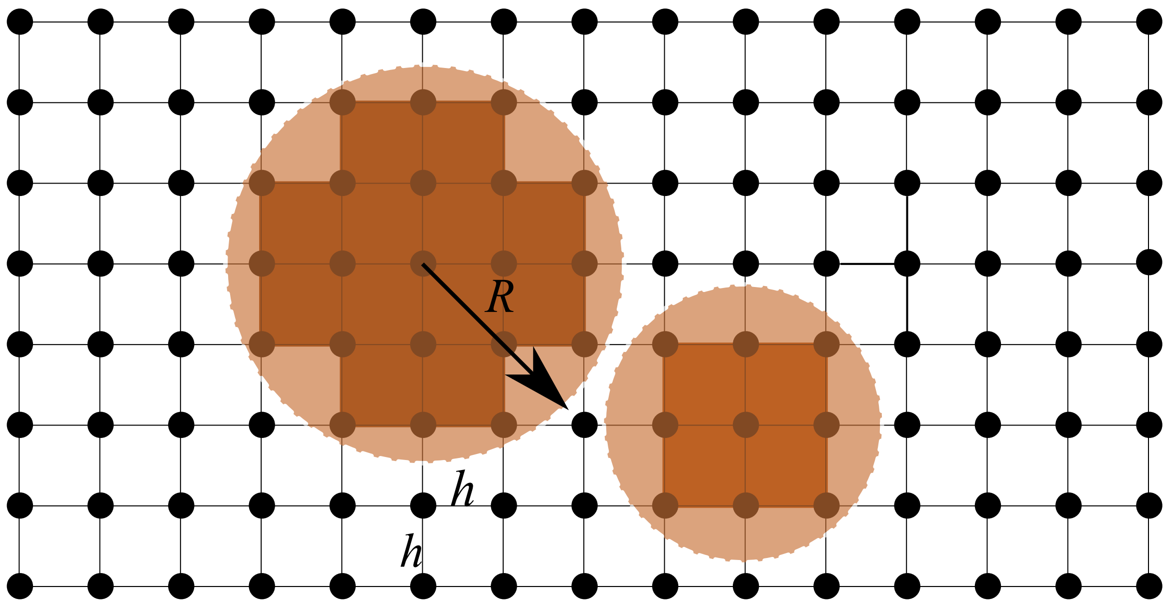

Figure 6.6 Discretisation of solid grains in LBM grid. Shows the step-wise representation of circular disks in the lattice.

6.3.2 Collapse in fluid: Flow evolution

Two-dimensional plane-strain LBM-DEM simulations of granular column collapse are performed by varying the initial aspect ratio of the column from 0.2 to 6. The normalized final run-out distance is computed as $\Delta L = (L_f - L_0)/L_0$. Similar to dry granular collapse, the duration of collapse is normalised with a criticial time $\tau_c = \sqrt{H/g}$. Where, H is the initial height of the granular column and g is the acceleration due to gravity. Dry and buoyant analyses of granular column collapse are also performed to understand the effect of hydrodynamic forces on the run-out distance.

Snapshots of flow evolution of a granular column collapse with an initial aspect ratio of 0.4 is shown in figure 6.7. The failure begins at the toe end of the column, and the fracture surface propagates into the column at an angle of about 50°, similar to dry column. For the short column, the failure is due to collapse of the flanks. Once the material is destabilisied, the granular mass interacts with the surrounding fluid resulting in formation of turbulent vortices. These vortices interact with the grains at the surface, resulting in irregularities on the free surface. Force chains can be observed in the static region of collapse, which indicates the flow can be described using a continuum theory. As the granular material ceases to flow, force chains develop at the flow front, revealing consolidation of the granular mass resulting in increase in strength.

The evolution of run-out with time for a short column (a = 0.4) is presented in figure 6.8a. The dry column exhibits longer run-out distance in comparison to the submerged column. The collapse of a dry column using DEM represents a collapse in vacuum, without any influence of drag forces or viscosity of air. A LBM-DEM simulation of a granular column collapse using the kinematic viscosity of air is performed to compare the dry column with the collapse in air. It can be observed that both the "dry" condition and the collapse in air show almost the same run-out behaviour. However, the collapse in fluid (water) results in a much shorter run-out distance. The granular mass in fluid has the buoyant mass, in contrast to the dry density. A dry granular collapse with the buoyant unit weight is performed to understand the effect of buoyancy on the run-out behaviour. The dry column with buoyant unit weight also exhibits longer run-out behaviour than the collapse in fluid. However, due to decrease in the initial potential energy, the run-out observed in the buoyant condition is shorter than the dry condition. The column collapse in fluid takes longer to evolve when submerged in water, which might be due to the development of large negative porewater pressure that is generated during the shear failure along the fracture surface. The large negative pore pressure has to be dissipated before the granular mass above the fracture surface can collapse and flow. The shorter run-out distance in the fluid case, in comparison with the dry and buoyant conditions, shows that the collapse in fluid is significantly affected by the hydrodynamic drag force acting on the soil grains. The evolution of height H/L is presented in **??**. Since the failure of the column is only at the flank, the central static region remains unaffected. Hence, the final height of the column is the same in dry and submerged conditions.

(a) $t = 0\tau_c$

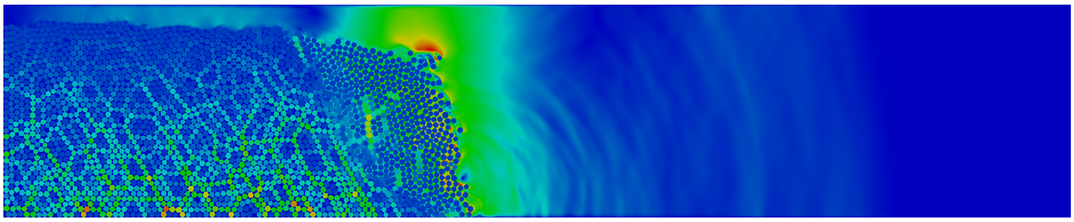

(b) $t = 1\tau_c$

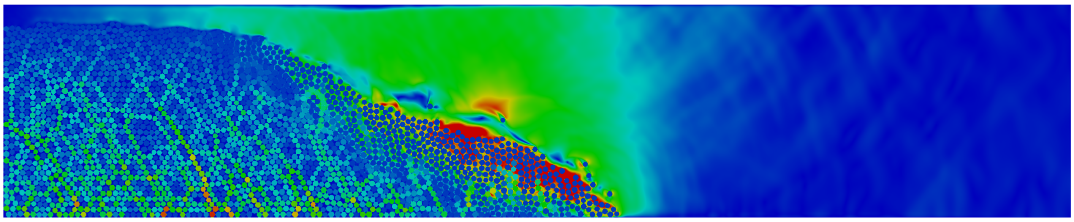

(c) $t = 3\tau_c$

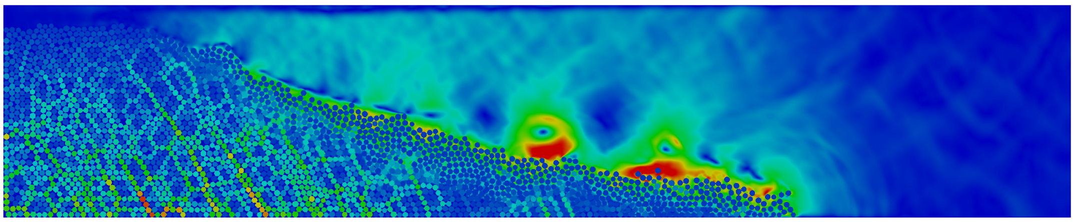

(d) $t = 6\tau_c$

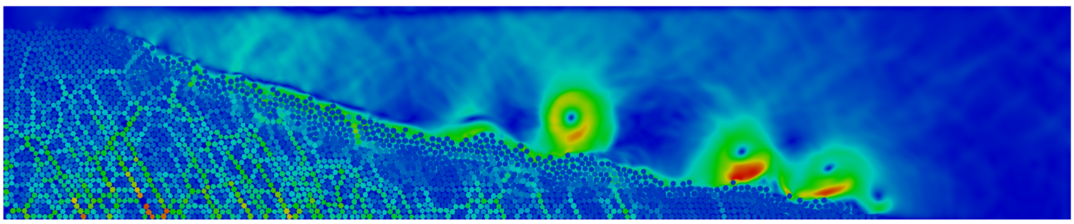

(e) $t = 8\tau_c$

Figure 6.7 Flow evolution of a granular column collapse in fluid (a = 0.4). Shows the velocity profile of fluid due to interaction with the grains (red - higher velocity).

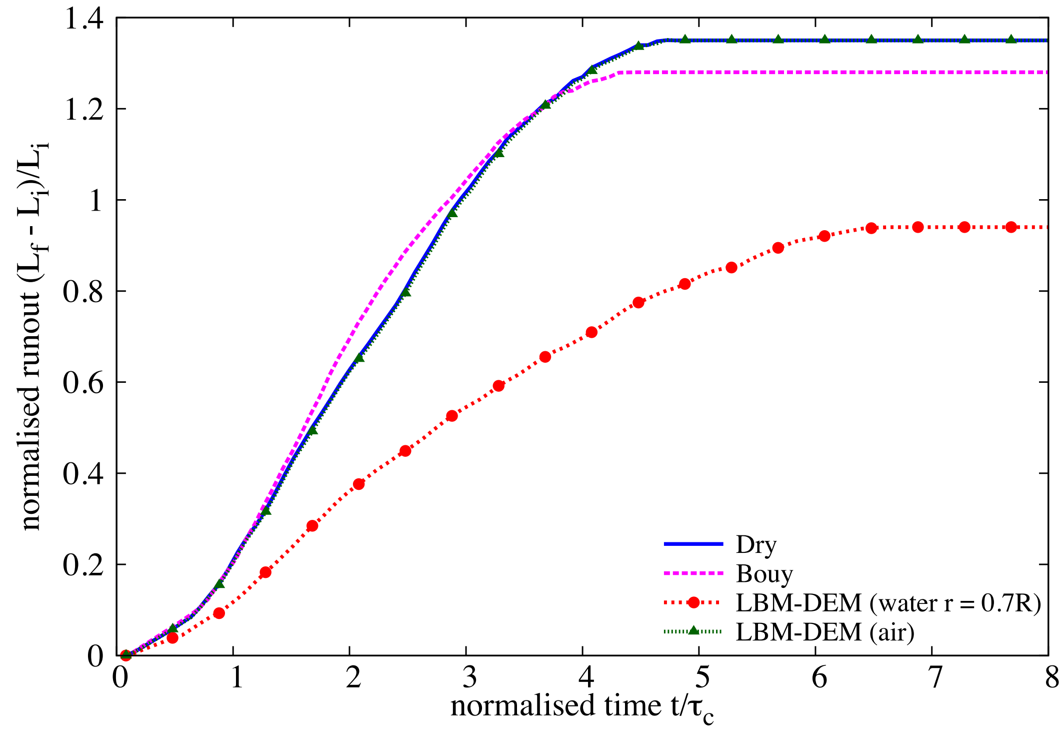

(a) Evolution of run-out with time

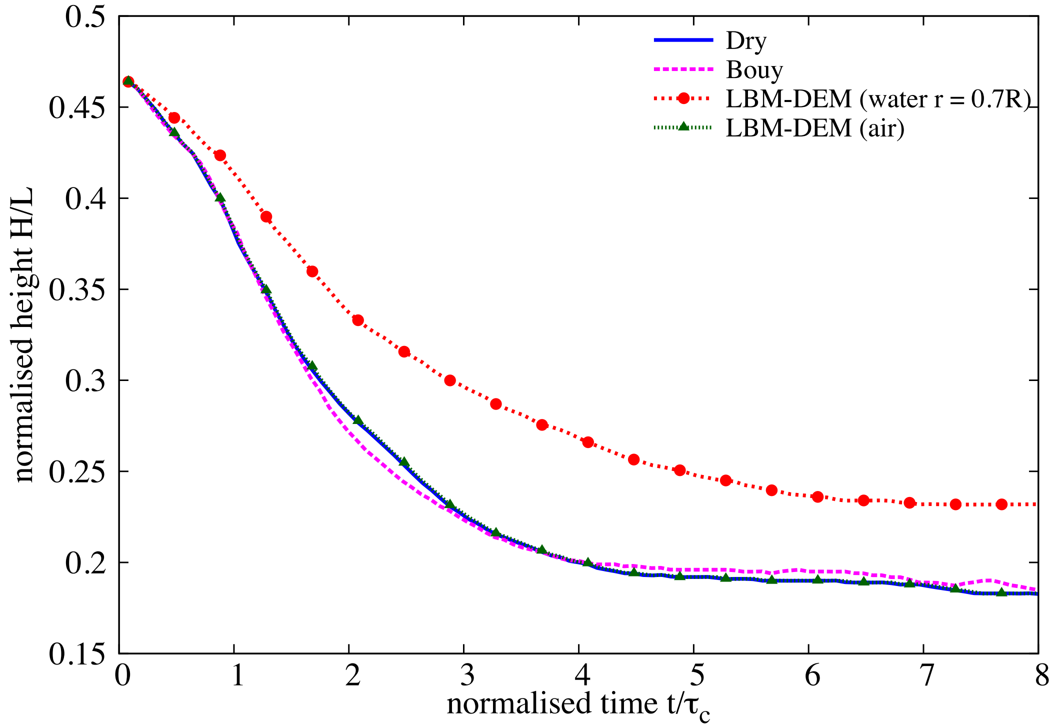

(b) Evolution of height with time

Figure 6.8 Evolution of height and run-out with time for a column collapse in fluid (a = 0.4)

The evolution of normalised kinetic energy with time for a column with an initial aspect ratio of 0.4 is shown in figure 6.9. It can be observed that the peak kinetic energy is attained later in the submerged condition than the dry collapse. This can be attributed to the time required to overcome the negative pore pressure generated during the shear along the fracture surface. For short columns the critical time τ_c is controlled by the vertical kinetic energy. The amount of kinetic energy in submerged case is significanlty lower than the dry condition. Also, the potential energy evolution (see figure 6.10) shows a significant influence of the hydrodynamic forces on the amount of material destabilised during the collapse. The drag forces reduces and slows down the amount of material that undergo collapse resulting in shorter run-out distance for short columns.

Snapshots of the flow evolution of a granular column collapse with an initial aspect ratio of 4 is shown in figure 6.10. For a tall column, the collapse mechanism changes. The entire column is involved in the collapse. The height of the static region, which is below the fracture surface, is shorter than the total height of the column. This results in a free-fall of grains above the fracture surface. As the grains experience free-fall they interact with the surrounding fluid. However, no vortices are observed during the initial stage of collapse. In the second phase, when the grains reach the base, the vertical acceleration gained during the free-fall is converted to horizontal kinetic energy. As the grains are ejected horizontally, the free surface of the granular mass interacts with the fluid resulting in formation of the turbulent vortices. Unlike short columns, these vortices have significant influence on the mass distribution along the run-out. Heaps of granular material can be observed in front of each vortices. The number of vortices formed during a collapse is found to be proportional to the amount of material destabilised, i.e., the length of free-surface interacting with the fluid influences the number of vortices generated during the collapse. The reappearance of force chains at $t = 6\tau_c$ &$8\tau_c$ indicates the granular mass is consolidating resulting in an increase in the shear strength.

The time evolution of the run-out and height of a tall column (a=4) is presented in figure 6.11a and figure 6.11b, respectively. Similar to the short column, the run-out observed in the dry condition is much longer than that observed in submerged condition. Also, the evolution of run-out is slower in case of submerged condition, which indicates the influence drag force on the run-out evolution. The height of the column is significantly affected by the hydrodynamic forces (see figures 6.11b and 6.12), which reduces the amount of material destabilised during collapse.

The evolution of kinetic energies with time for aspect ratio 4 is presented in figure 6.13. Even during the free-fall stage, the peak vertical energy is delayed in the case of fluid, which shows the influence of the viscosity on the flow evolution. Almost half of the kinetic energy that is available in the case of dry granular collapse is dissipated due to the drag force experienced by

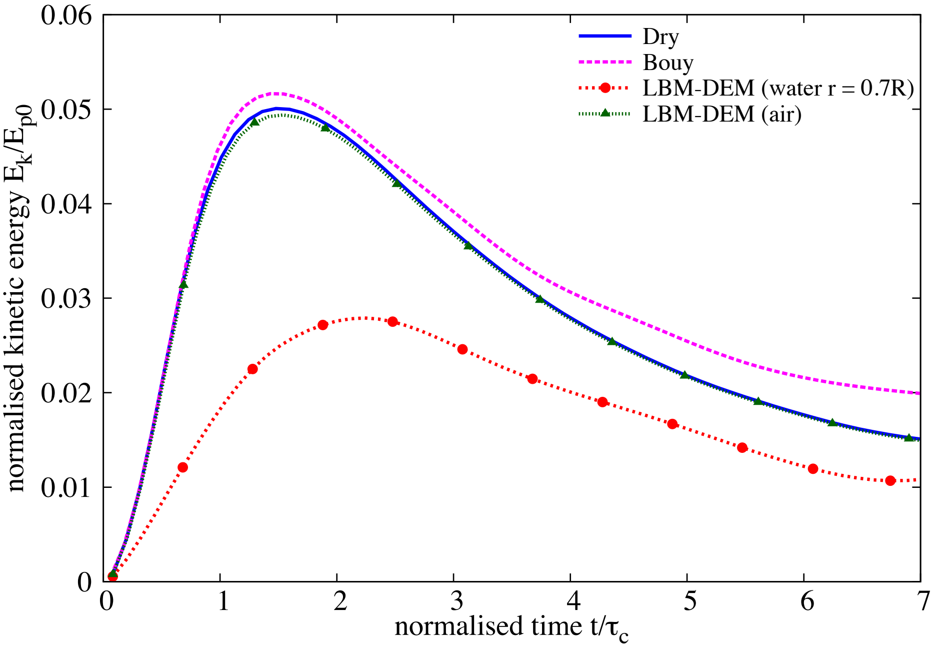

(a) Evolution of the total kinetic energy

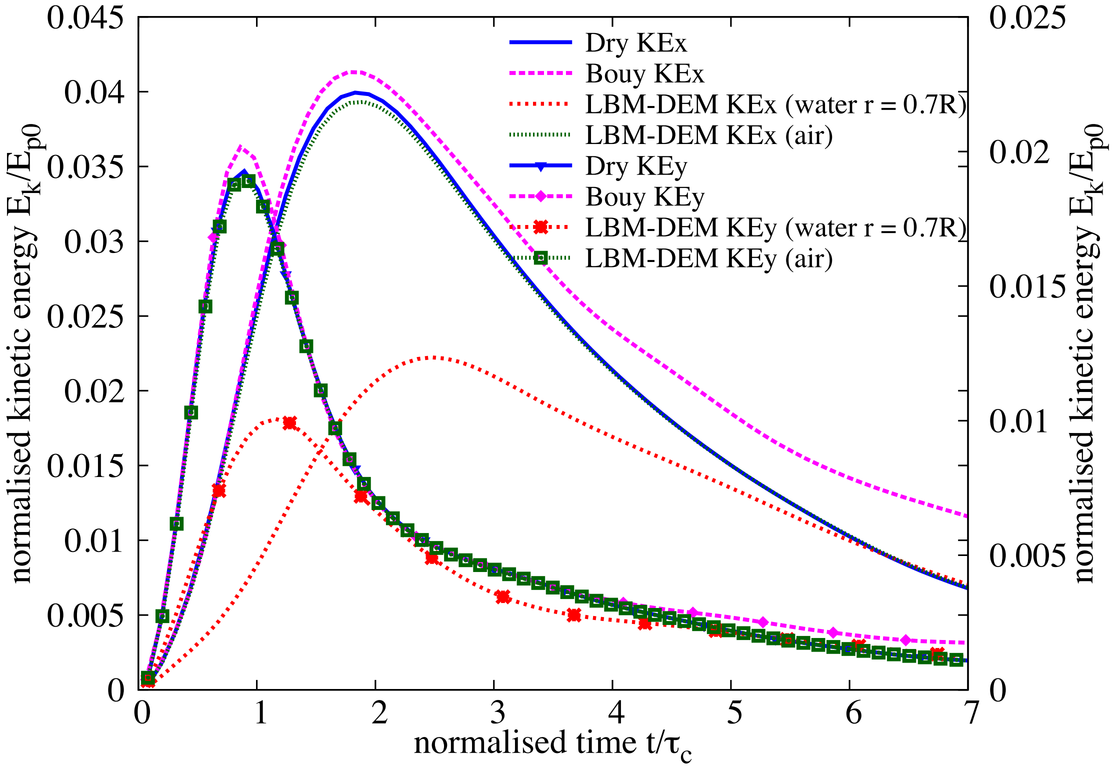

(b) Evolution of horizontal and vertical kinetic energies

Figure 6.9 Evolution of kinetic energies with time for a granular column collapse in fluid (a = 0.4)

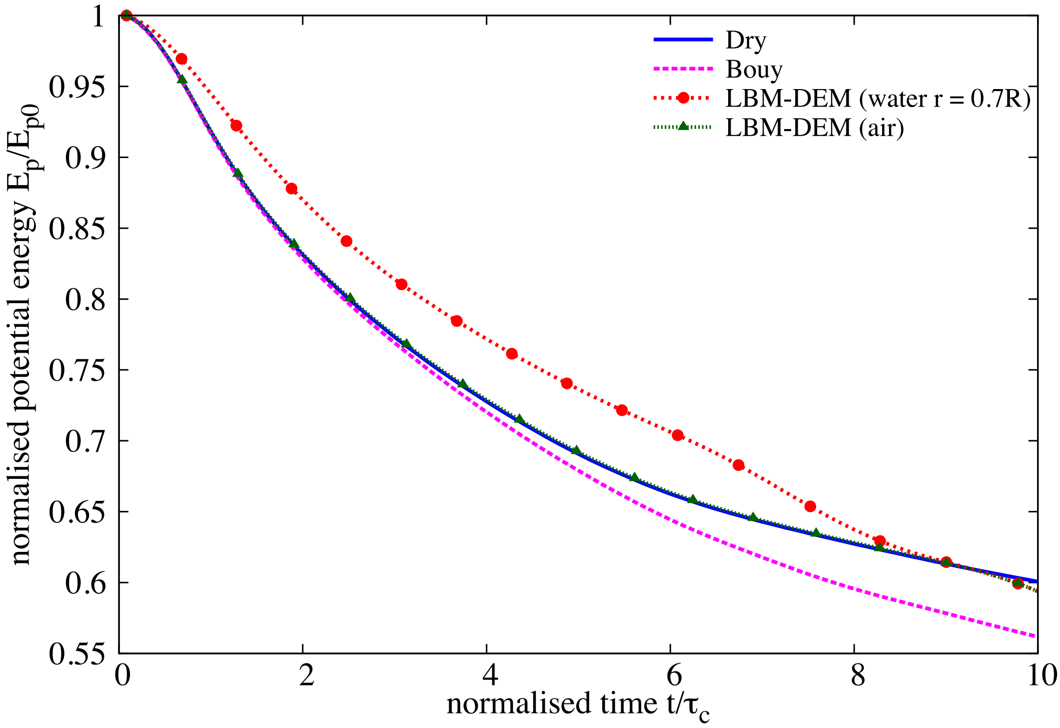

Figure 6.10 Evolution of the potential energy with time for a granular column collapse in fluid (a = 0.4)

the grains. This shows that the influence of viscous drag on the run-out evolution is significantly higher than the effect of lubrication.

The initial aspect ratio of the column is varied from 0.2 to 6. The final run-out distance as a function of the initial aspect ratio of the columnt is presented in figure 6.14a. For all aspect ratios, the run-out observed in the dry case is significantly higher than the submerged condition. For short columns, the run-out distance is found to be have a linear relationship with the initial aspect ratio of the column. A power law relation is observed between the run-out and the initial aspect ratio of the column. The normalised final height as a function of the initial aspect ratio of the column is presented in figure 6.14b. It can be observed that the final collapse height is much higher in fluid than the dry condition. The drag force on the granular column reduces the amount of collapse, resulting in a shorter run-out distance. The drag force seems to have a predominant influence on the run-out behaviour than the lubrication effect in fluid.

$$\frac{L_f - L_0}{L_0} \propto \begin{cases} a, & a \lesssim 2.7 \\ a^{2/3}, & a \gtrsim 2.7 \end{cases} \tag{6.5}$$

$t = 0\tau_c$

$t = 1\tau_c$

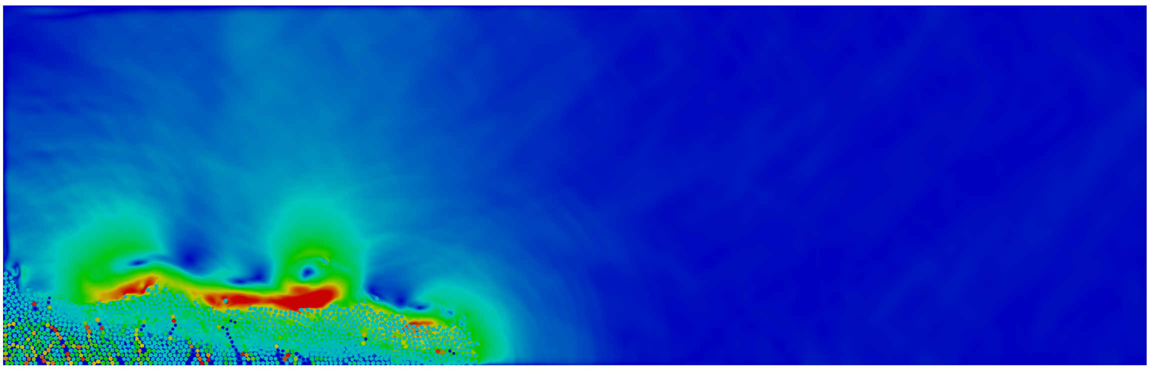

$t = 3\tau_c$

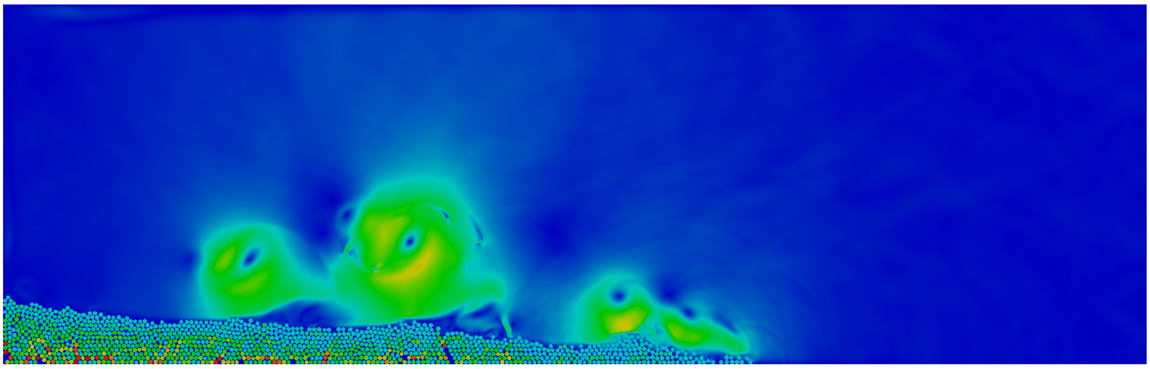

$t = 6\tau_c$

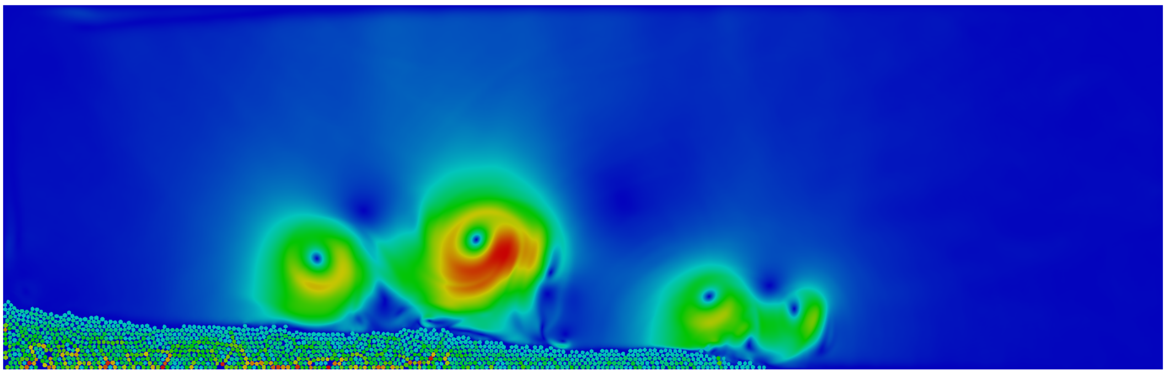

$t = 8\tau_c$

Figure 6.10 Flow evolution of a granular column collapse in fluid (a = 4). Shows the velocity profile of fluid due to interaction with the grains (red - higher velocity).

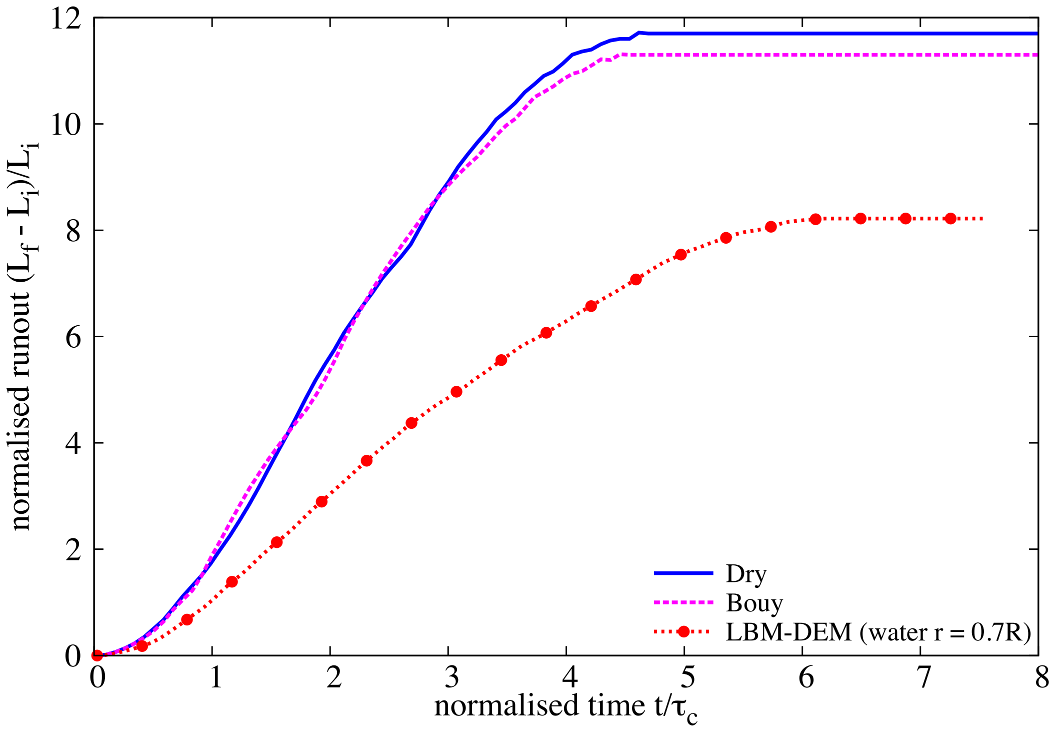

(a) Evolution of run-out with time

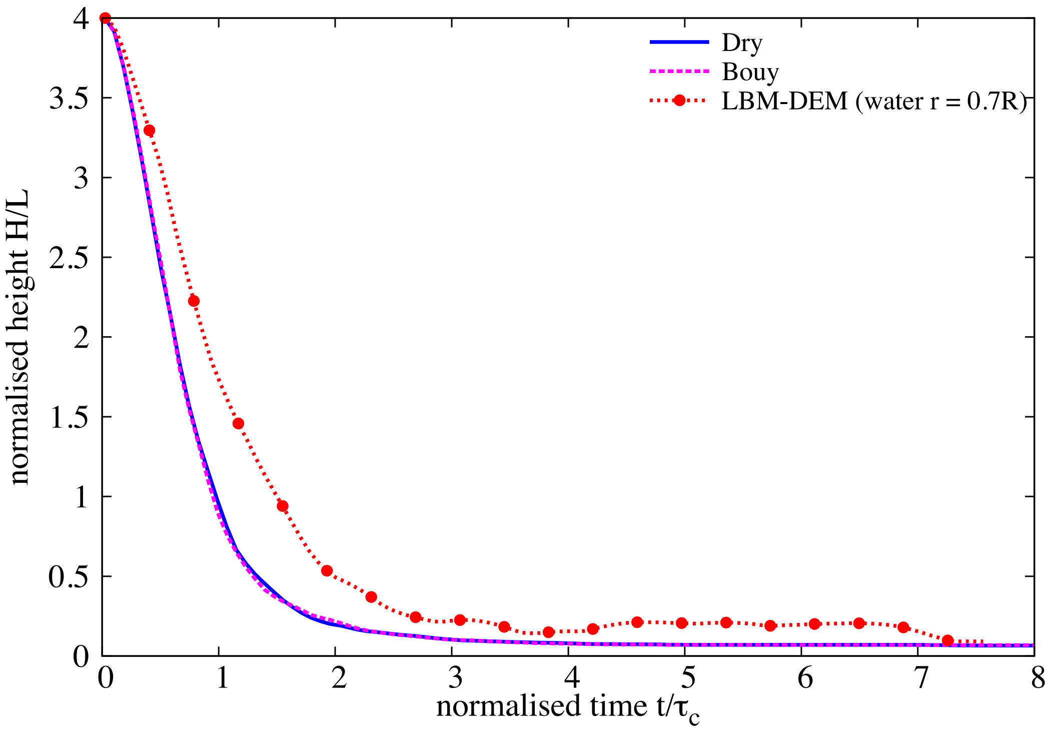

(b) Evolution of height with time

Figure 6.11 Evolution of run-out and height with time for a column collapse in fluid (a = 4)

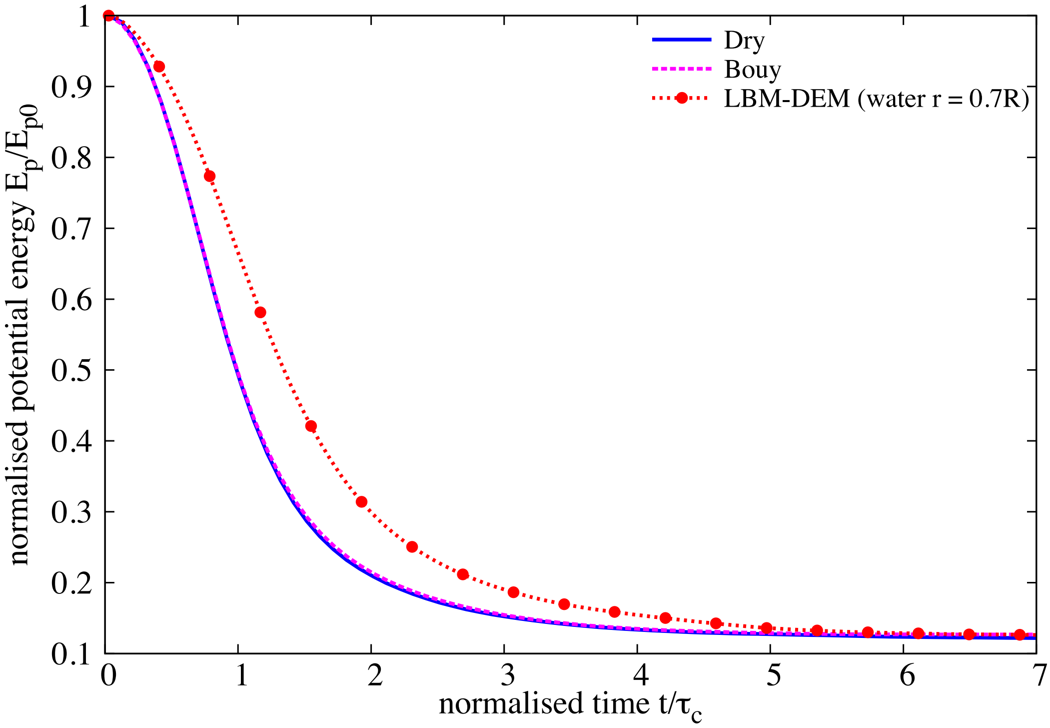

Figure 6.12 Evolution of the potential energy with time for a granular column collapse in fluid (a = 4)

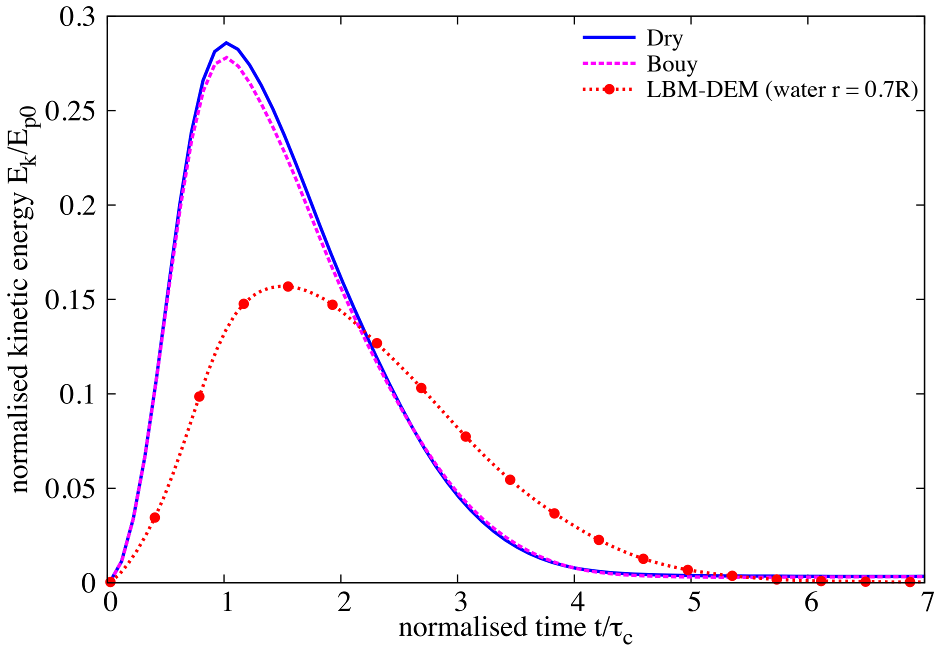

(a) Evolution of the total kinetic energy

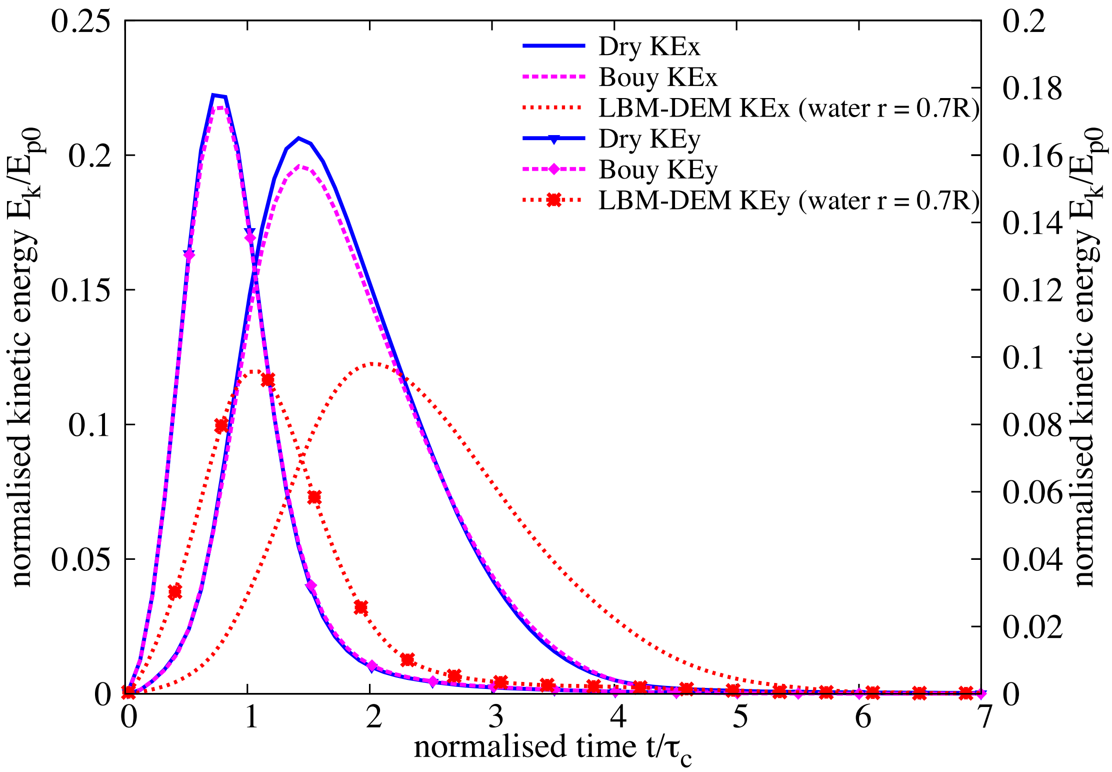

(b) Evolution of horizontal and vertical kinetic energies

Figure 6.13 Evolution of kinetic energies with time for a granular column collapse in fluid (a = 4)

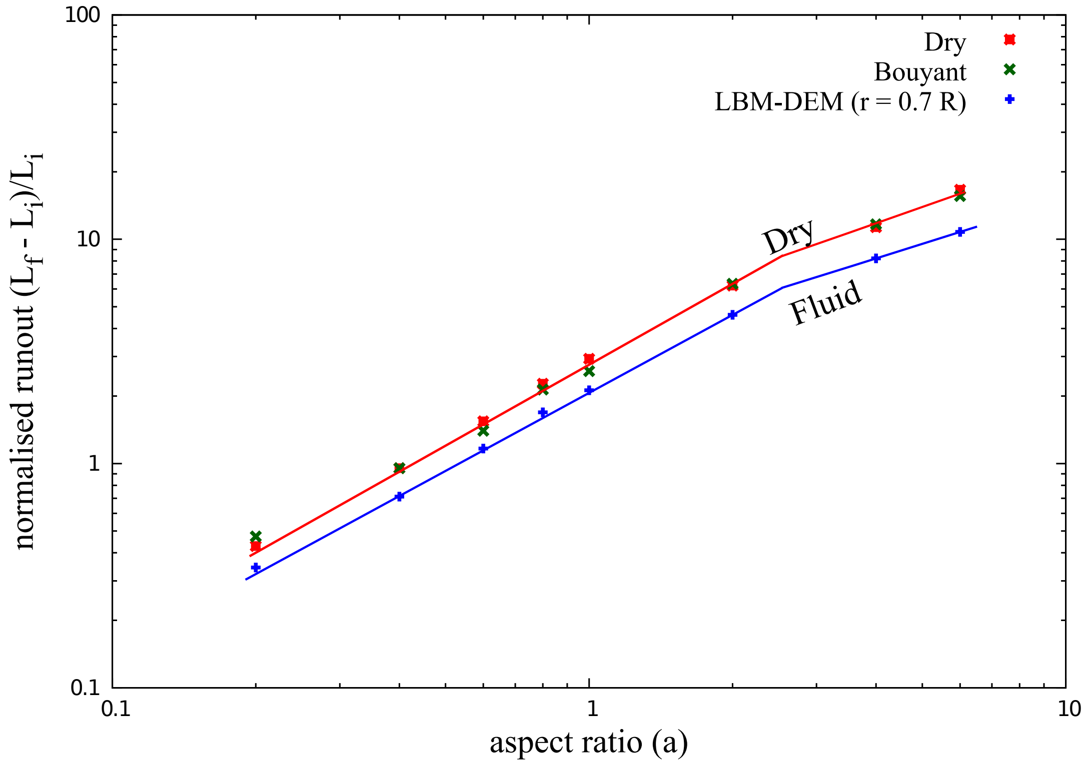

(a) Normalised final run-out distance for columns with different initial aspect ratios. Comparison of dry and submerged granular column collapse.

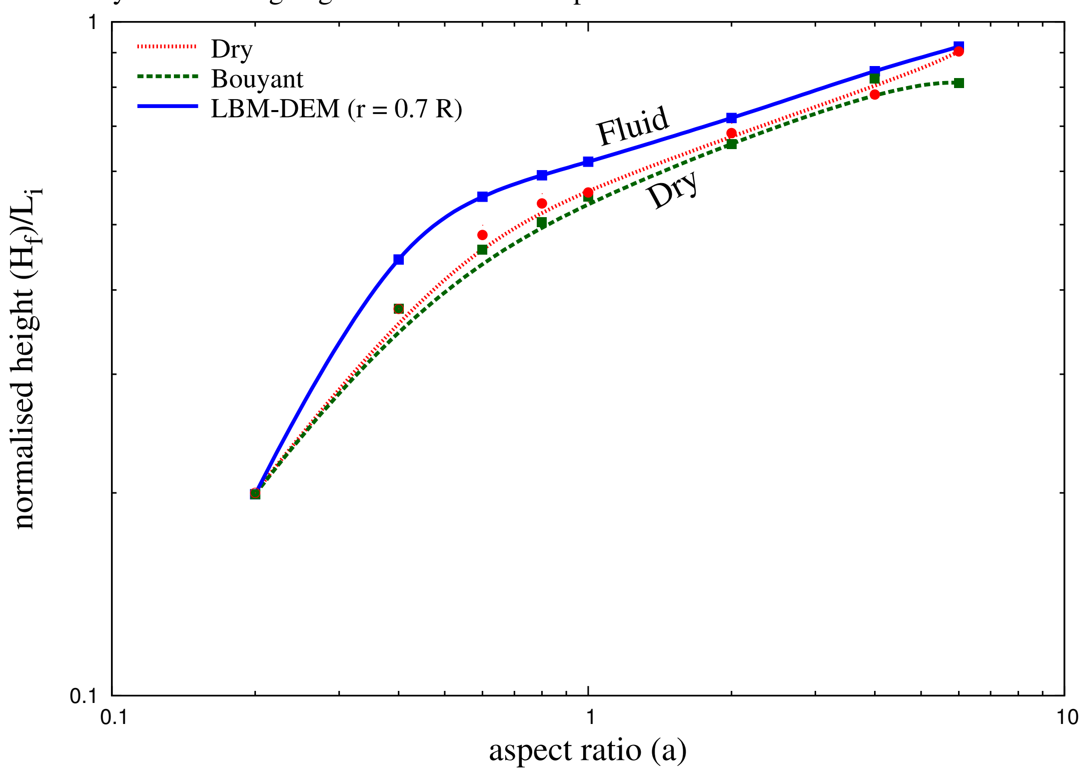

(b) Normalised final collapse height for columns with different initial aspect ratios. Comparison of dry and submerged granular column collapse.

Figure 6.14 Normalised final collapse run-out and height for columns with different initial aspect ratios.

6.3.3 Effect of permeability

Topin et al. (2011) observed development of large negative pore pressure during dispersion of grains. The rate of dissipation of the negative pore pressure is directly proportional to the permeability of the granular assembly. In the previous section, the evolution of run-out with the initial aspect ratio is studied using a constant hydrodynamic radius r = 0.7 R. In order to understand the effect of permeability on the run-out behaviour, the hydrodynamic radius r is varied from 0.7 R through 0.95 R. Increase in hydrodynamic radius decreases the permeability of the granular assembly resulting in longer duration for the dissipation of negative pore pressure.

The normalise run-out for different hydrodynamic radius for a granular column collapse with an initial aspect ratio of 0.8 is presented in figure 6.15. The run-out increases with decrease in the permeability, which is equivalent to increase in the hydrodynamic radius. An increase in the hydrodynamic radius from 0.7 to 0.95 R, increases the normalised run-out by 25%. However, even under very low permeable condition (r = 0.95 R), the run-out observed in fluid is shorter than the dry and the buoyant conditions.

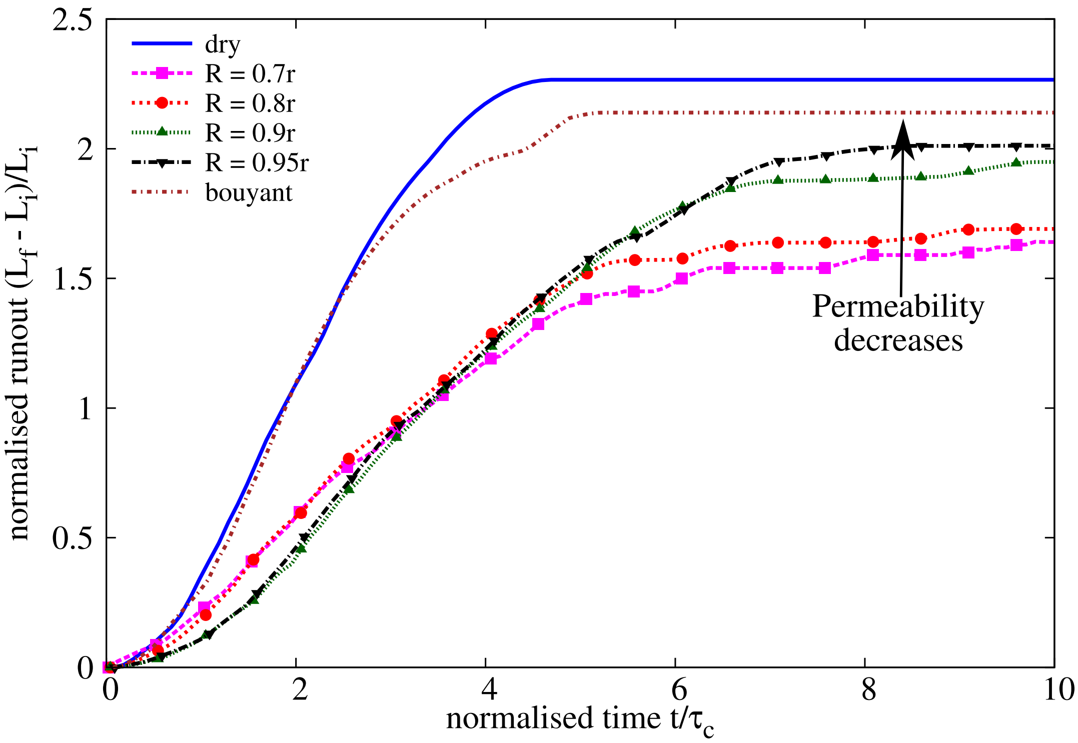

Figure 6.15 Effect of permeability on the evolution of run-out for a column collapse in fluid (a = 0.8)

At high permeability (r = 0.7 R), the evolution of run-out at the initial stage is quicker, which means that the negative pore-pressure that is developed during the shearing along the fracture surface is dissipated faster. Even though the negative pore-pressure is dissipate, due to the development of negative pore-pressure the evolution of run-out in fluid is slower than its dry counterpart. The rate of dissipation decreases with decrease in the permeability. This can be observed by a flatter slope in the run-out evolution with decrease in permeability. figure 6.16 shows the distribution of pore-pressure in high and low permeable granular media. At the same time $t = \tau_c$, the high permeable (r = 0.7 R) shows smaller negative pore-pressure in comparison to large negative pore-pressures observed in the shearing zone for low permeable column (r = 0.9 R). This shows that not only does it take longer time for the pore-pressure to dissipate with decrease in permeability, the negative pore-pressure developed in the low permeable condition is almost twice that of high permeable case (see figure 6.16b).

Although low permeable granular columns take longer duration for the run-out to evolve, the final run-out distance is found to be much longer than high permeable condition. figure 6.17 shows that the potential energy available for the flow for low permeable column is 20% smaller than the collapse of high permeable granular column. The kinetic energy evolution (see figure 6.18) shows that the low permeable column has a wider peak kinetic energy distribution in comparison to a sharp peak observed in high permeable condition. This indicates the influence of lubrication, i.e., hydroplaning of the granular flow in low permeable conditions. The evolution of horizontal kinetic energy reveals that the peak kinetic energy is sustained longer as the permeability of the granular material decreases (see figure 6.18b). Although, the peak kinetic energy is smaller in the low permeability case, the hydroplaning of the flowing granular mass results in longer run-out distance. A high positive pore-pressure is observed at the base of the granular flow in low permeability condition (figure 6.19b) indicating the occurrence of hydroplaning. The evolution of local packing density shows a drop in the packing density at low permeability (see figure 6.20). The drop in the value of packing density between $t = 2\tau_c$ and $t = 3\tau_c$ corroborates with the duration of hydroplaning during which large amount of water in entrained at the flow front.

High permeable column shows lower water entrainment, which indicates that at highly permeable flows the drag force acting on the soil grains predominates over the lubrication effect. In both low permeable and high permeable granular flows, the granular material consolidates at the final stage of the flow. This can be observed as the packing density increases at the final stage due to grains settling and expulsion of entrained water. The final deposit profile for both low and high permeability condition is shown in figure 6.21. High permeable collapse show a more parabolic (convex) deposit profile in contrast to the more concave profile observed in low permeability condition. The observation of hydroplaning in low permeable condition may be due to the distribution of the granular mass at the flow front. Instigation of hydroplaning is controlled by the balance of gravity and inertia forces at the debris front and is suitably

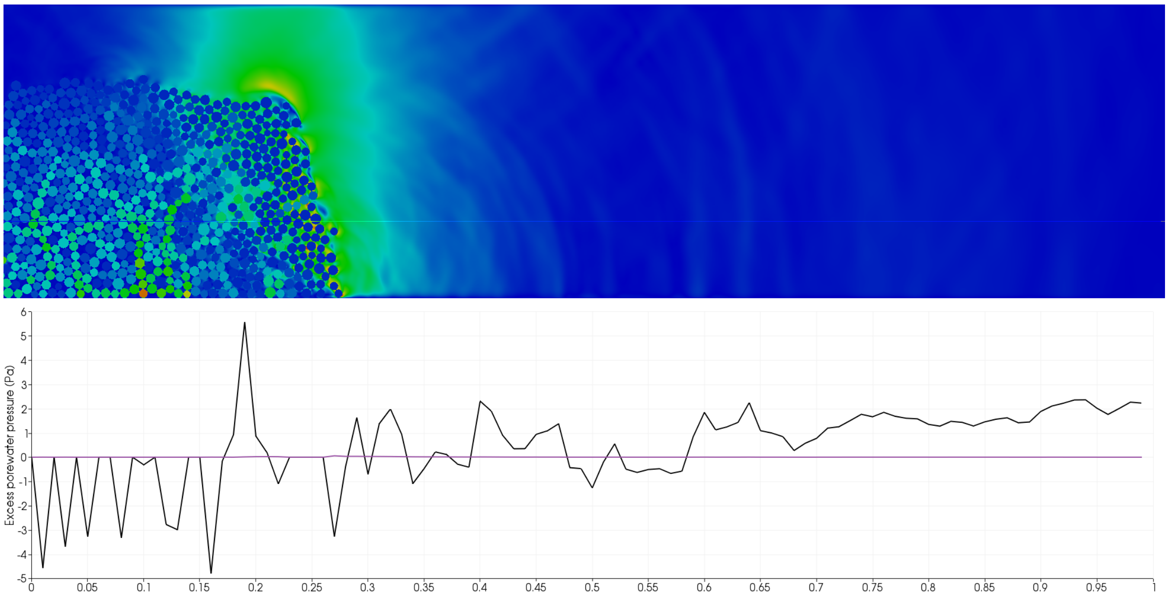

(a) High permeability (r = 0.7 R)

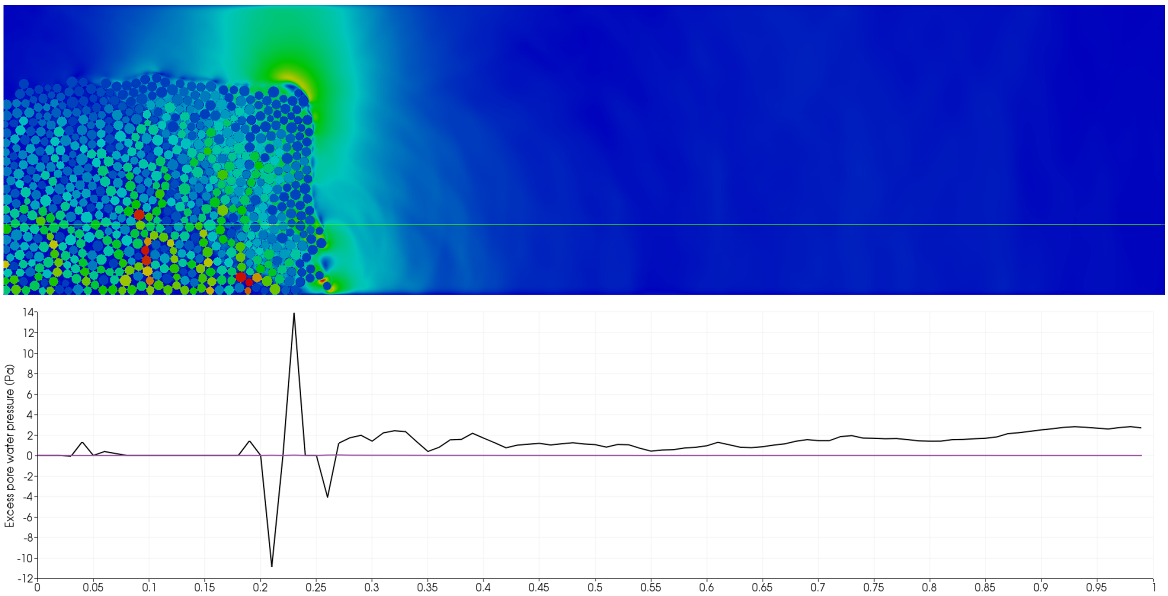

(b) Low permeability (r = 0.95 R)

Figure 6.16 Effect of permeability on the excess pore water pressure distribution for a granular column collapse in fluid (a = 0.8 & dense packing) at $t = \tau_c$

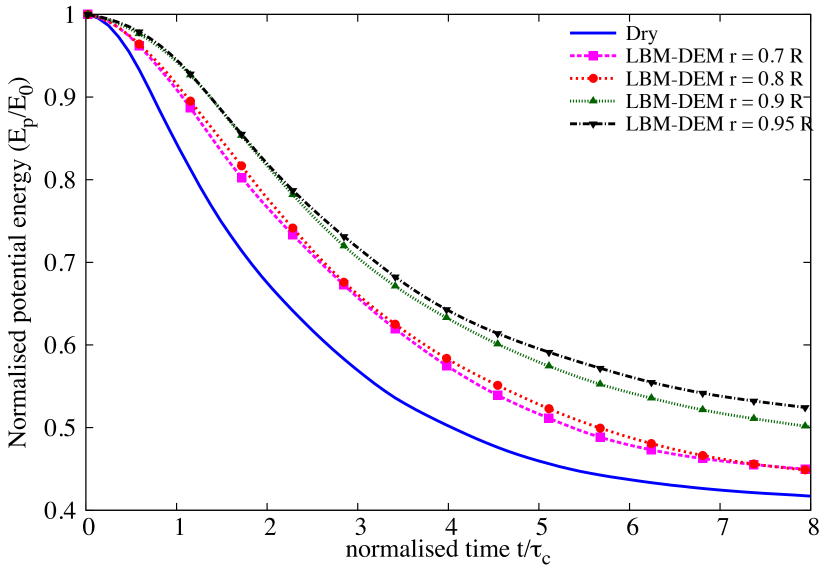

Figure 6.17 Effect of permeability on the evolution of the potential energy with time for a granular column collapse in fluid (a = 0.8)

characterized by the densimetric Froude's number:

$$Fr_d = \frac{U}{\sqrt{(\frac{\rho_d}{\rho_w} - 1)gH\cos\theta}} \tag{6.6}$$

where U is the average velocity of sliding mass, ρ_p and ρ_w are the densities of soil and water, respectively, H is the thickness of the sliding mass, g is acceleration due to gravity and θ represents the slope angle. Harbitz (2003); Mohrig and Ellis (1998) observed hydroplaning above a critical value of densimetric Froude's number of 0.4. A Fr_d value of 0.427 is observed for low permeable flow (r = 0.95 R), which indicates the occurrence of hydroplaning. Where as a $Fr_d = 0.273$ is observed for high permeable granular flow indicating absence of hydroplaning, the low permeable collapse is predominated by the viscous drag force resulting in a parabolic profile and shorter run-out distance.

The normalised final run-out distance as a function of the initial aspect ratio of the column is presented in figure 6.22. For all aspect ratios, the dry condition yields the longest run-out distance. For a given aspect ratio, the dry collapse acquires the highest kinetic energy due to the lack of fluid dissipation during vertical collapse. This extra kinetic energy is high enough to propel the heap, in-spite of a high frictional dissipation, over a distance that is longer than the run-out distance in the fluid regime. In submerged condition, for the same aspect ratio, the kinetic energy available for spreading is lower and the dissipation due to viscous drag is higher, thus leading to a much shorter run-out distance.

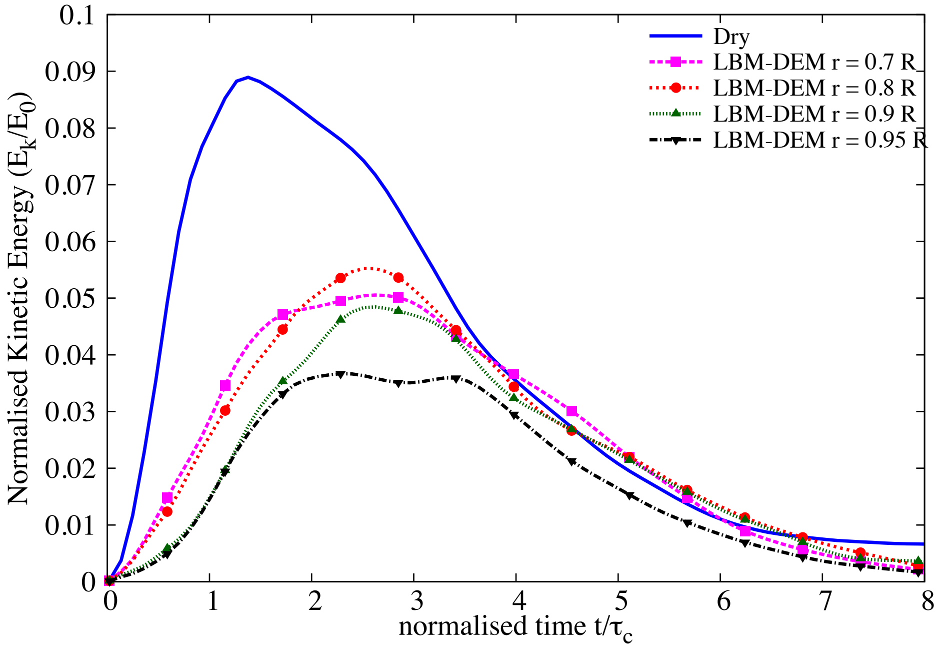

(a) Evolution of the total kinetic energy

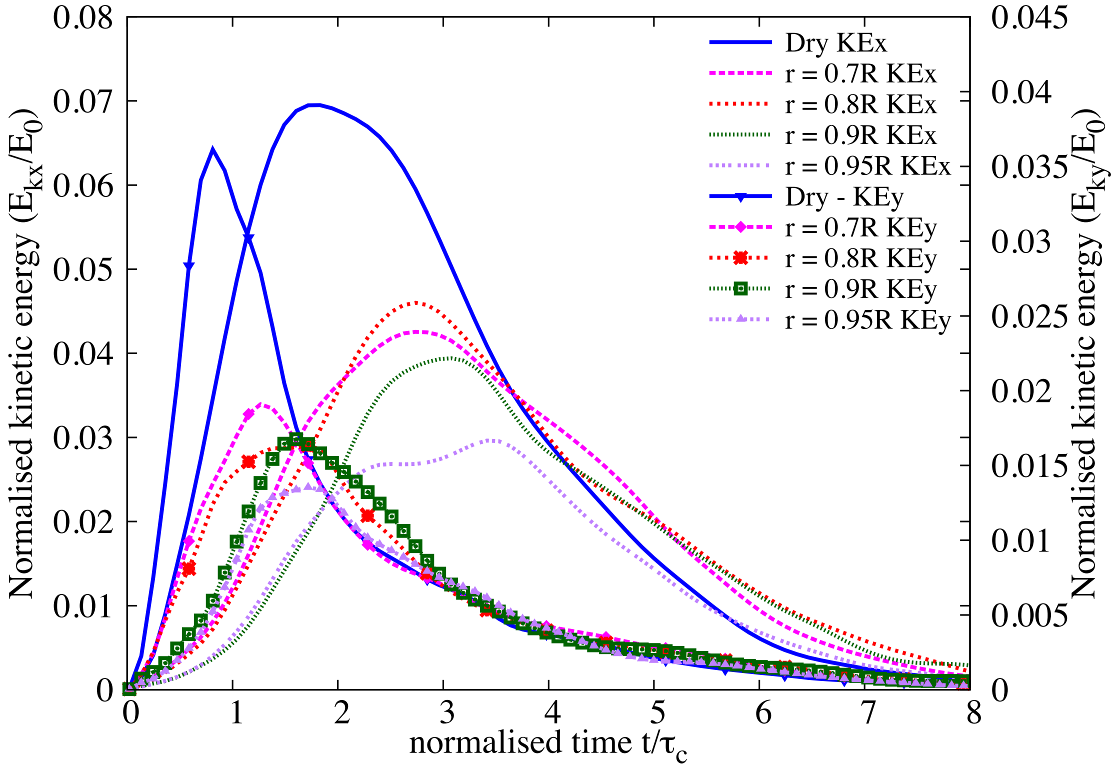

(b) Evolution of horizontal and vertical kinetic energies

Figure 6.18 Effect of permeability on the evolution of kinetic energies with time for a granular column collapse in fluid (a = 0.8)

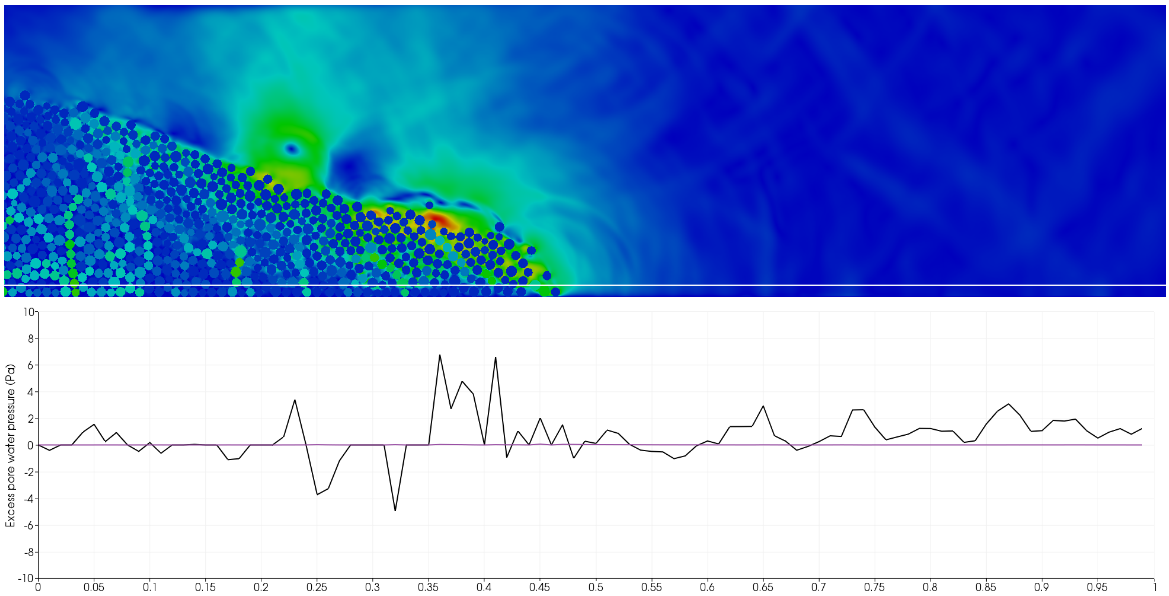

(a) High permeability (r = 0.7 R)

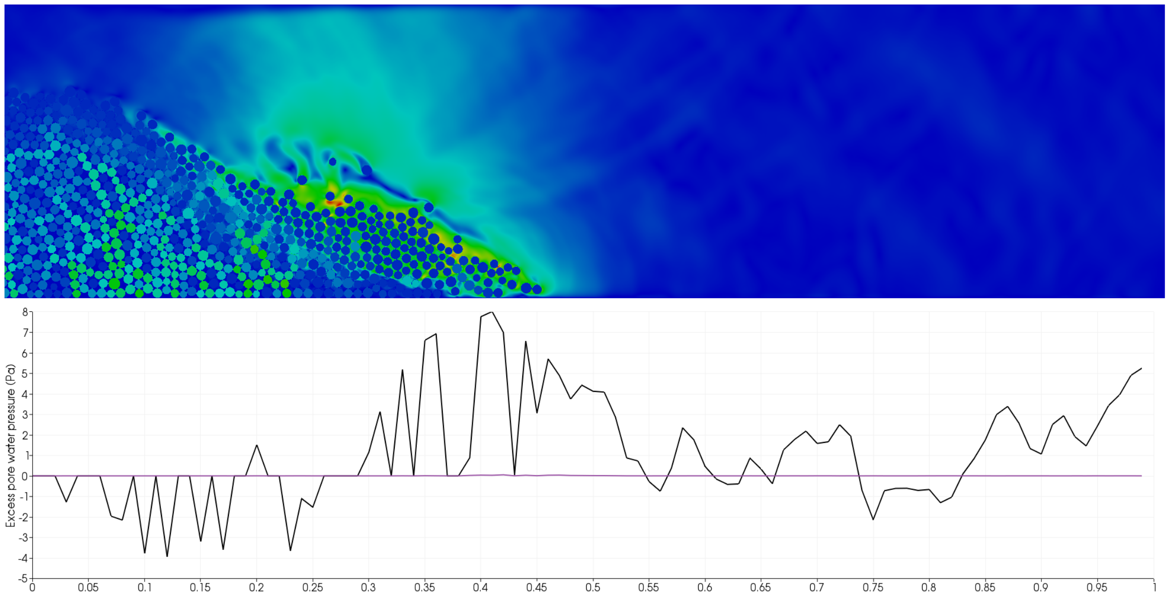

(b) Low permeability (r = 0.95 R)

Figure 6.19 Effect of permeability on the excess pore water pressure distribution for a granular column collapse in fluid (a = 0.8 & dense packing) at $t = 2\tau_c$

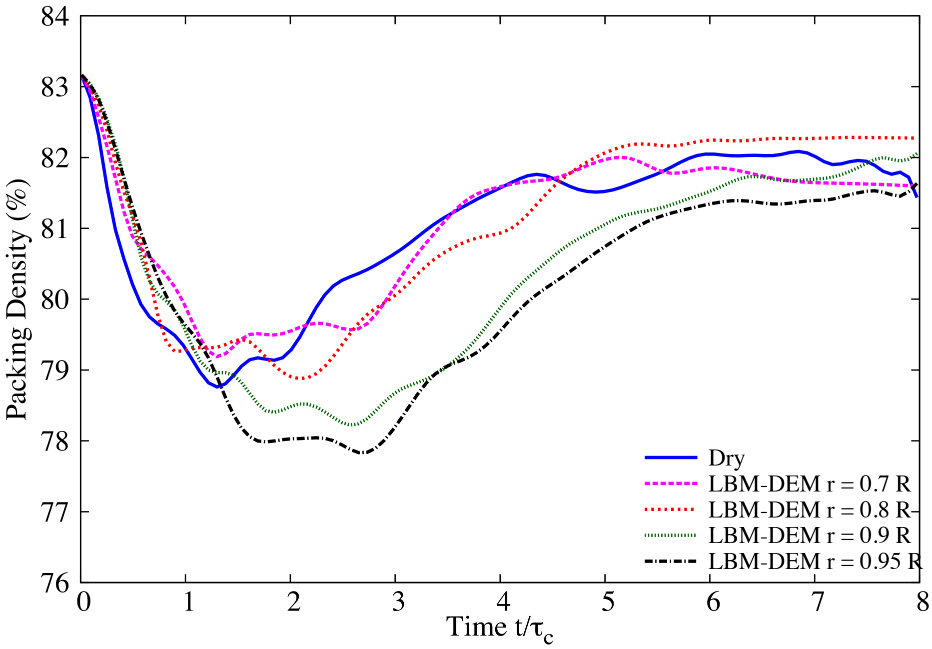

Figure 6.20 Effect of permeability on the evolution of packing density for a granular column collapse in fluid (a = 0.8 & dense initial packing)

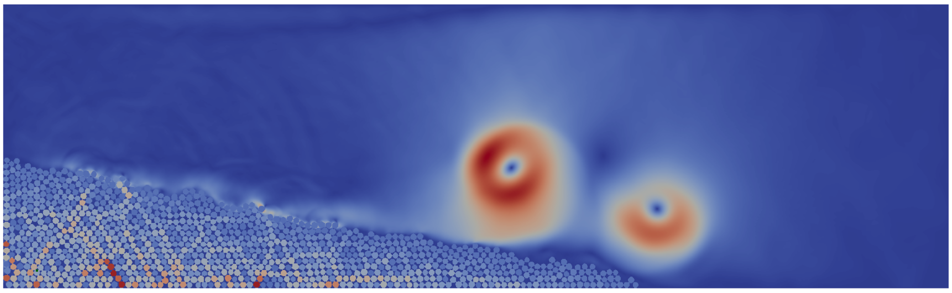

(a) High permeability (r = 0.7 R)

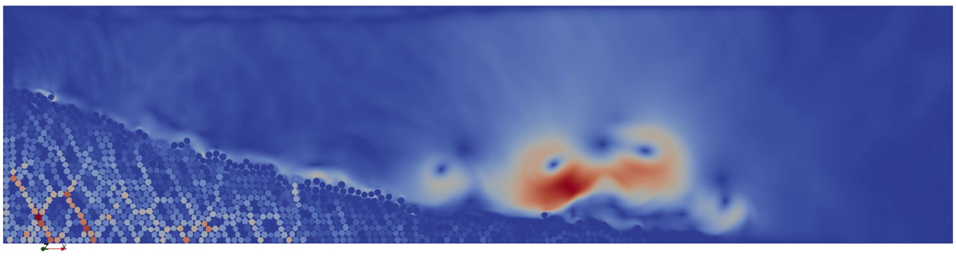

(b) Low permeability (r = 0.95 R)

Figure 6.21 Effect of permeability on the deposit morphology of a granular column collapse in fluid (a = 0.8)

For short columns, with decrease in permeability the run-out distance increases, however, the run-out distance is not higher than the dry condition. At higher aspect ratios, decrease in permeability from r = 0.8 R to r = 0.9 R does not have a significant influence on the run-out behaviour. This can be attributed to the turbulent nature of the granular flows for tall columns. The run-out behaviour is a result of transformation of (part of) the initial potential energy to the peak kinetic energy, which in turn controls the subsequent run-out along the plane. The run-out distance is plotted as a function of the normalised peak kinetic energy in figure 6.23. For the same aspect ratio, the peak kinetic energy is higher in the case of dry column. This represents grain inertial regime in dry granular collapse, which indicates that a part of the potential energy, in the presence of the fluid, is dissipated during the vertical collapse due to viscous friction. In all regimes, the run-out distance increases as a power law $L_f \propto KE_{max}^{\gamma}$. For the same value of peak kinetic energy, the run-out distance in fluid is longer than the dry column collapse. Also, with decrease in permeability the run-out distance increases for the same peak kinetic energy.

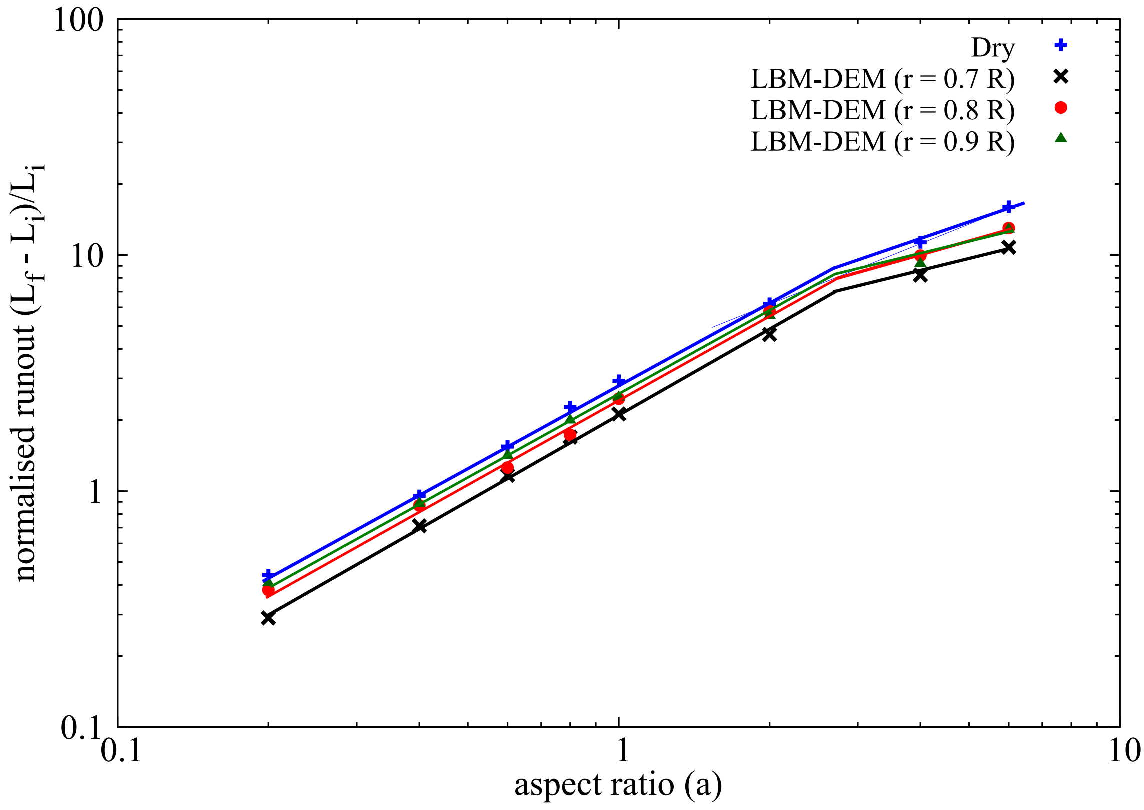

Figure 6.22 Normalised final run-out distance for columns with different initial aspect ratios. Comparison of dry and submerged granular column collapse for different hydrodynamic radius (0.7R, 0.8R and 0.9R).

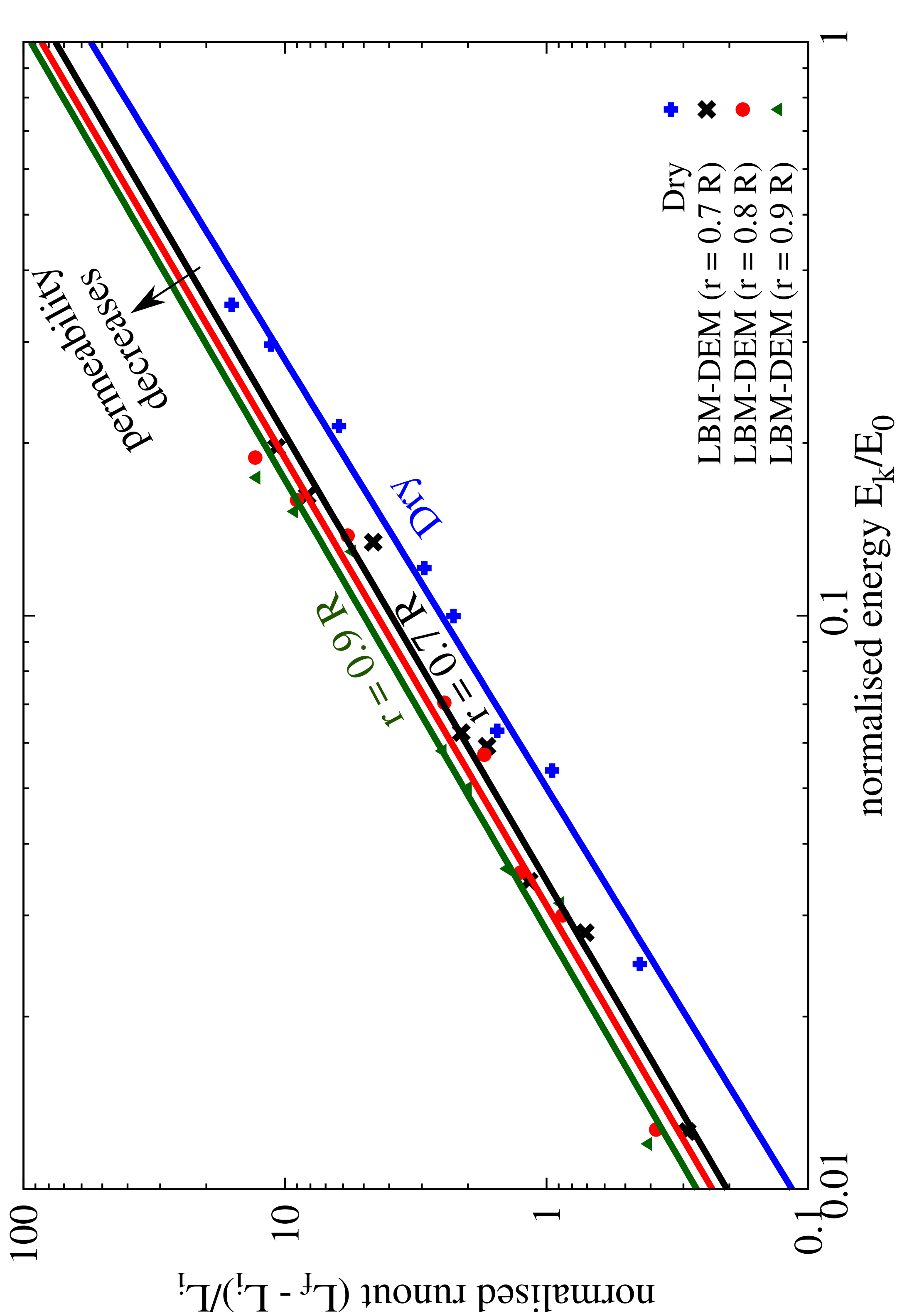

Figure 6.23 Normalised final run-out distance for columns as a function of peak kinetic energy. Comparison of dry and submerged granular column collapse for different hydrodynamic radius (0.7R, 0.8R and 0.9R).

6.3.4 Effect of initial packing density

Rondon et al. (2011) observed that the loose packings flow rapidly on a time scale proportional to the initial height and results in longer run-out distance in comparison to the dense packing. Hydroplaning occurs above a critical Froude's number of 0.4. The Froude's number is inversely related to the thickness of the flow and its density. Hence, for the same thickness of flow, a loose granular column will experience more hydroplaning than a dense granular flow. This effect might result in longer run-out behaviour in fluid than the dry condition for the same initial aspect ratio. The initial density and the permeability of a 2D granular column with an initial aspect ratio of 0.8 is varied to understand their influence on the run-out behaviour. The run-out behaviour of the dense case (83% packing density), discussed in the previous section, is compared with a loose granular colum (79% packing fraction). The permeability is varied by changing the hydrodynamic radius from 0.7 R to 0.95 R.

The normalised run-out evolution with time for a loose initial packing (79% packing fraction) with different hydrodynamic radius 0.7 R, 0.8 R, 0.9 and 0.95 R. The run-out evolution of dry and a column with grains in suspension with an initial aspect ratio of 0.8 is also presented to understand the influence of hydrodynamic forces on the flow kinematics. Similar to dense granular column, the run-out distance increases with increase in the hydrodynamic radius (i.e., decrease in permeability). At low permeability (r = 0.9 and 0.95R), the run-out distance is longer than the dry condition. This shows that the lubrication effect in low permeability condition overcomes the influence of the drag force and the development of large negative pore pressure resulting in longer run-out distance. Although suspended granular mass experience high drag force and turbulent effects, the run-out evolves almost at the same rate in comparison with granular columns with high permeability. This shows the effect of permeability on the dissipation rate of negative pore pressure developed during the initial stage of collapse.

Figure 6.25 shows the development of negative pore pressure in low permeability (r = 0.95 R) and dissipation of negative pore pressure in high permability (r = 0.7 R) at the same time $t = \tau_c$. This difference in the quantity and the rate of dissipation of negative pore pressure results in difference in the rate of flow evolution. Low permeable column takes longer duration for the flow to evolve. As the flow progresses, low permeability of the granular column causes hydroplaning to occur at the base of the column resulting in longer run-out distance (see figure 6.26).

The evolution of potential energy with time reveals that at very low permeability (r = 0.95 R), the initial potential energy mobilised is smaller than at r = 0.9R. Also with decrease in permeability, the time required to dissipate the negative pore pressure increases. This results in a shorter run-out distance in the case of r = 0.95 R than r = 0.9 R. As the amount of material destabilised is small, which results in a thinner flow having a high Froude's number. However,

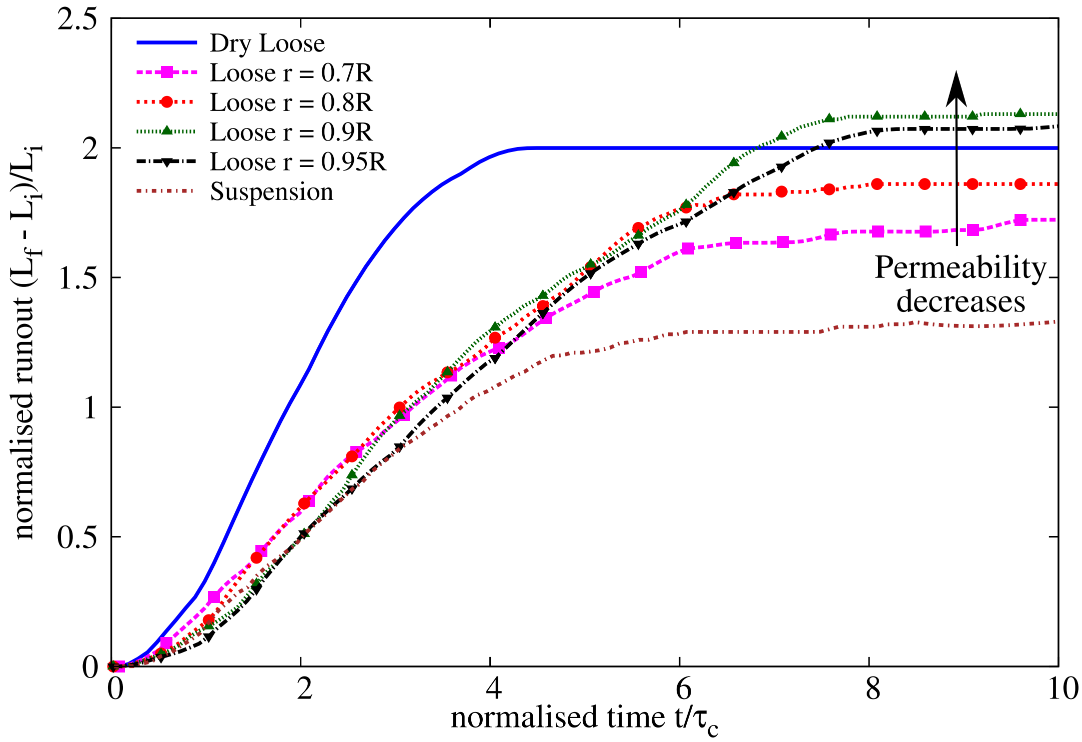

Figure 6.24 Effect of permeability on the evolution of run-out for a column collapse in fluid (a = 0.8 & loose packing)

the peak horizontal kinetic velocity observed in the case of r = 0.9 R is higher than r = 0.95 R (see figure 6.29b). A Froude's number of 0.59 for r = 0.9 R is observed in contrast to 0.46 for r = 0.94 R. Both values of hydrodynamic radius result in a Froude's number that indicates occurrence of hydroplaning. The difference in the amount of material destabilised for r = 0.95 R and the decreased effect of hydroplaning results in shorter run-out distance for r = 0.95 R in comparison to r = 0.9 R.

As the column collapses, water is entrained at the flow front. This can observed by decrease in the packing fraction during $t = 1\tau_c$ to $t = 3\tau_c$. As the flow progresses, the entrained water is expelled and the soil grains consolidate to reach a critical packing density at the end of the flow (see figure 6.28). The permeability (hydrodynamic radius) plays a crucial role in the rate of dissipation of the entrained water. As the permeability decreases, the water entrained at the flow front takes longer time to be dissipated resulting in lubrication of the flow at low permeability. This lubrication effect results in increased run-out for columns with low permeability.

The evolution grain trajectories with time is presented in figure 6.30 for low permeability (r = 0.95 R) and (r = 0.9 R). It can be observed that the column with high permeability shows a more parabolic (convex) final profile in contrast to the more concave profile observed in low permeability condition. This difference in the flow thickness results in higher value of

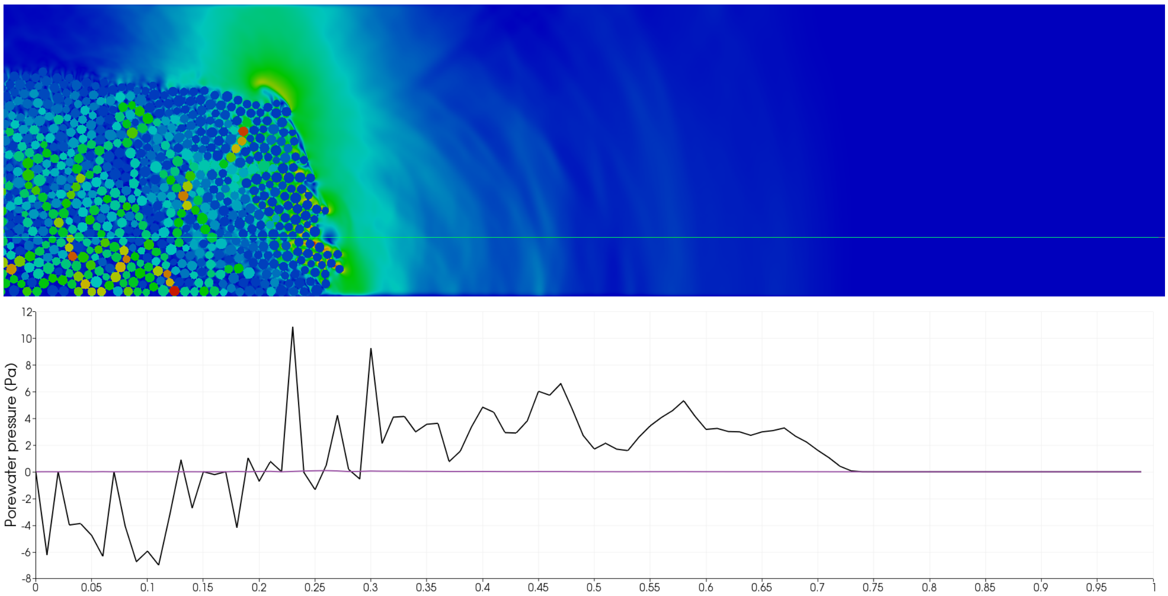

(a) High permeability (r = 0.7 R)

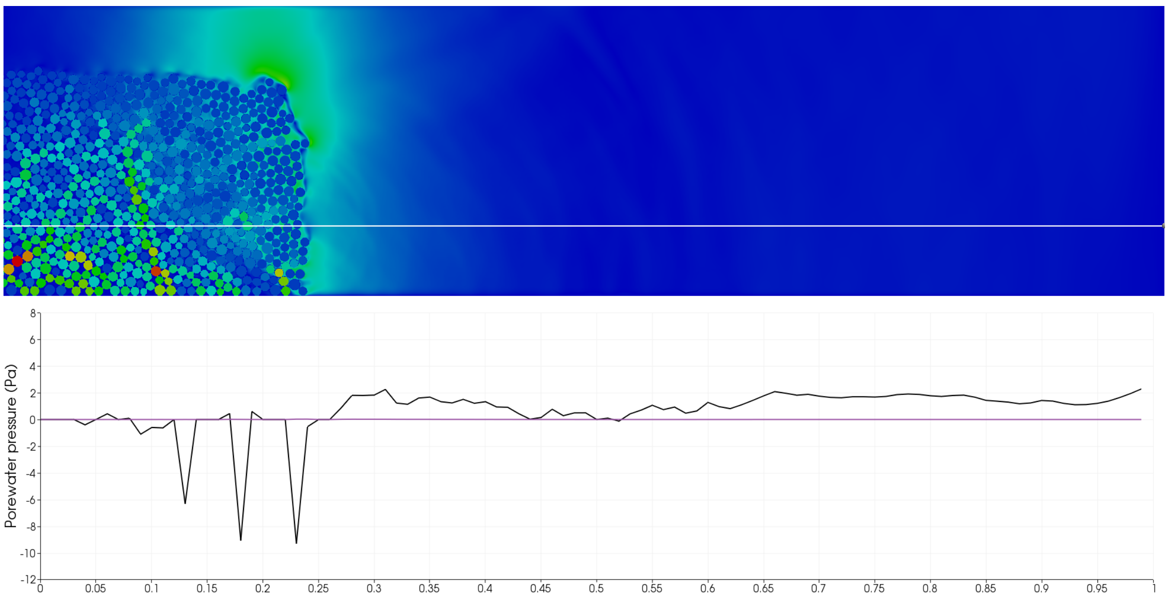

(b) Low permeability (r = 0.95 R)

Figure 6.25 Effect of permeability on the excess pore water pressure distribution for a granular column collapse in fluid (a = 0.8 & loose packing) at $t = \tau_c$

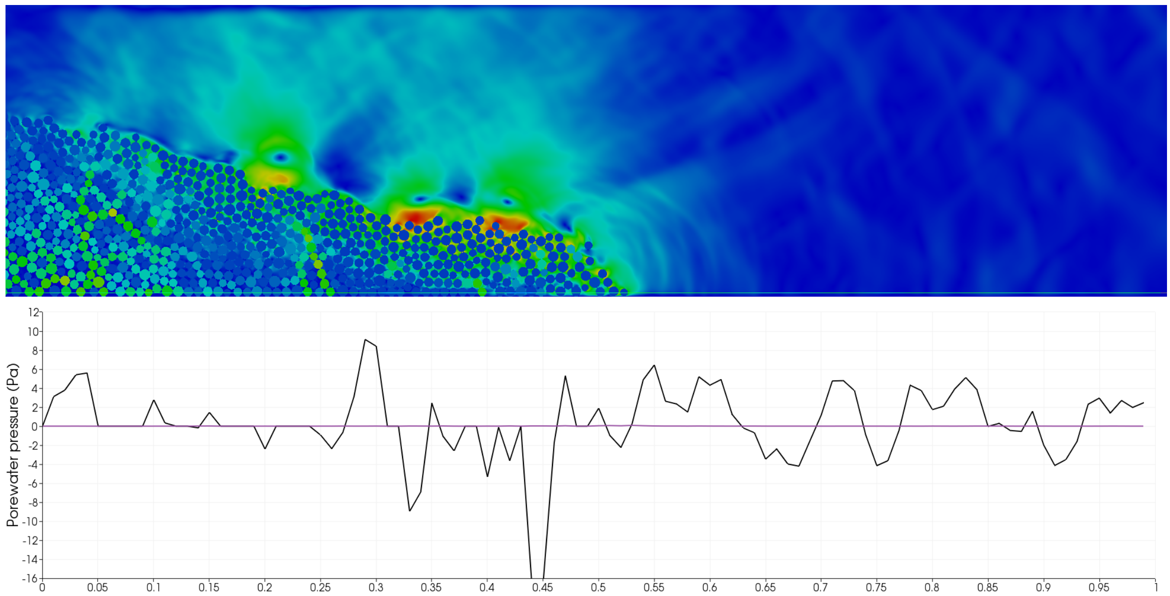

(a) High permeability (r = 0.7 R)

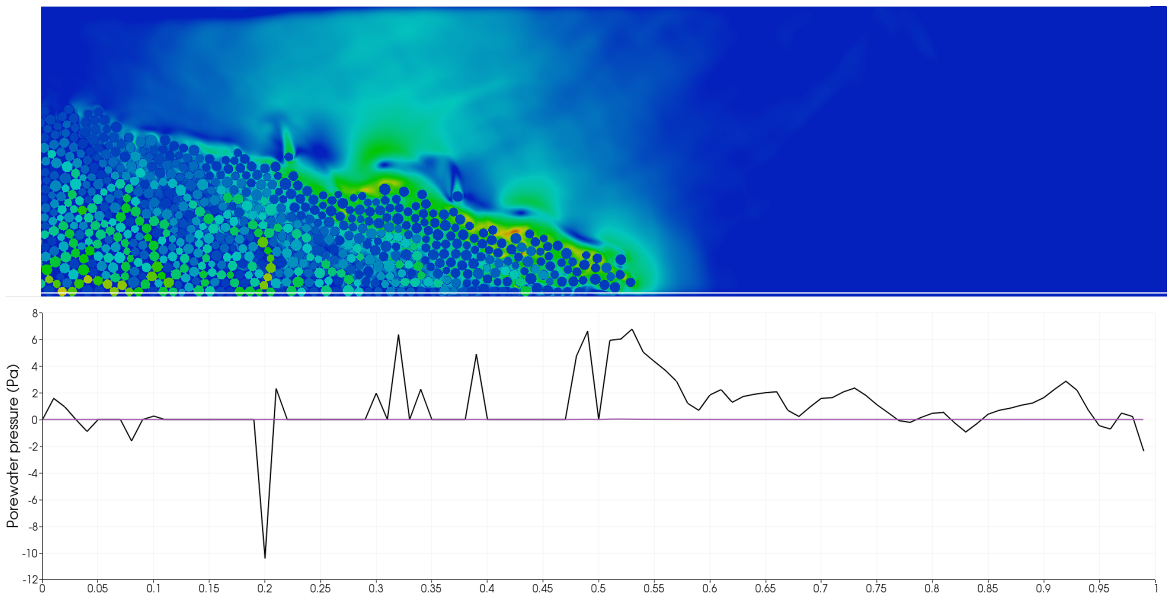

(b) Low permeability (r = 0.95 R)

Figure 6.26 Effect of permeability on the excess pore water pressure distribution for a granular column collapse in fluid (a = 0.8 & loose packing) at $t = 2\tau_c$

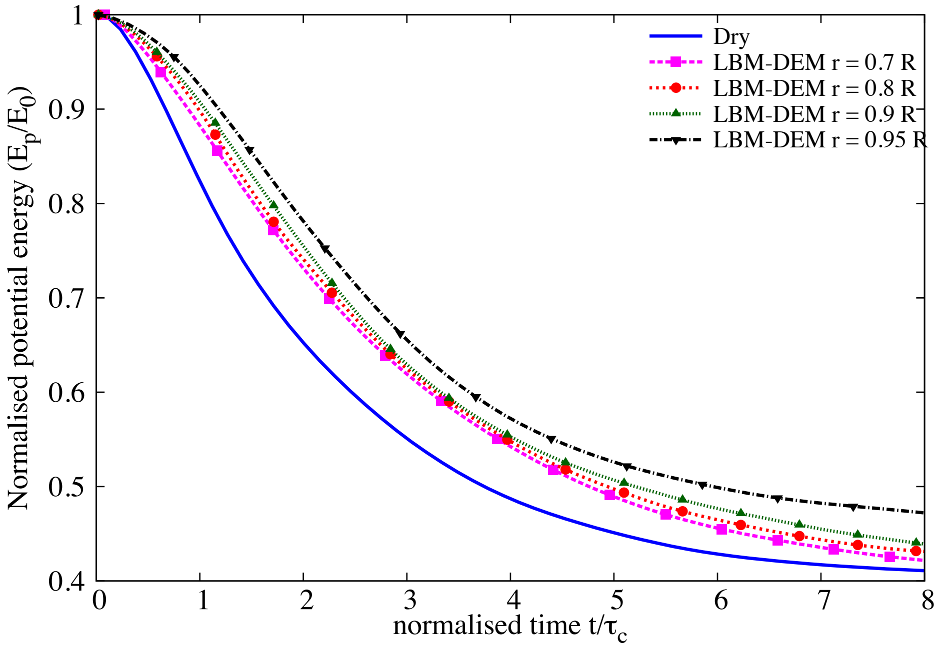

Figure 6.27 Effect of permeability on the evolution of the potential energy with time for a granular column collapse in fluid (a = 0.8 & loose packing)

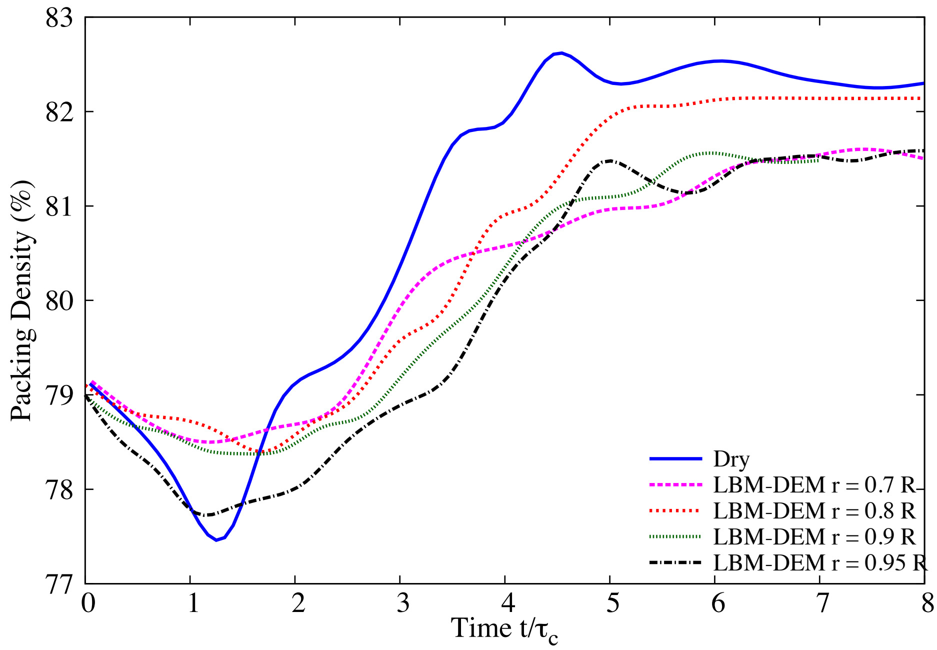

Figure 6.28 Effect of permeability on the evolution of packing density for a granular column collapse in fluid (a = 0.8 & loose initial packing)

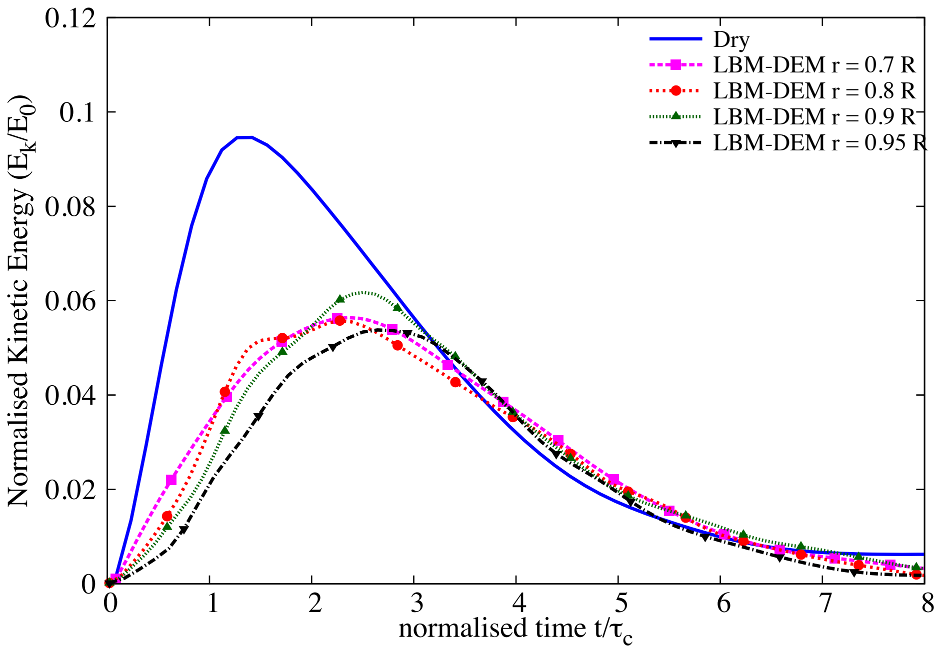

(a) Evolution of the total kinetic energy

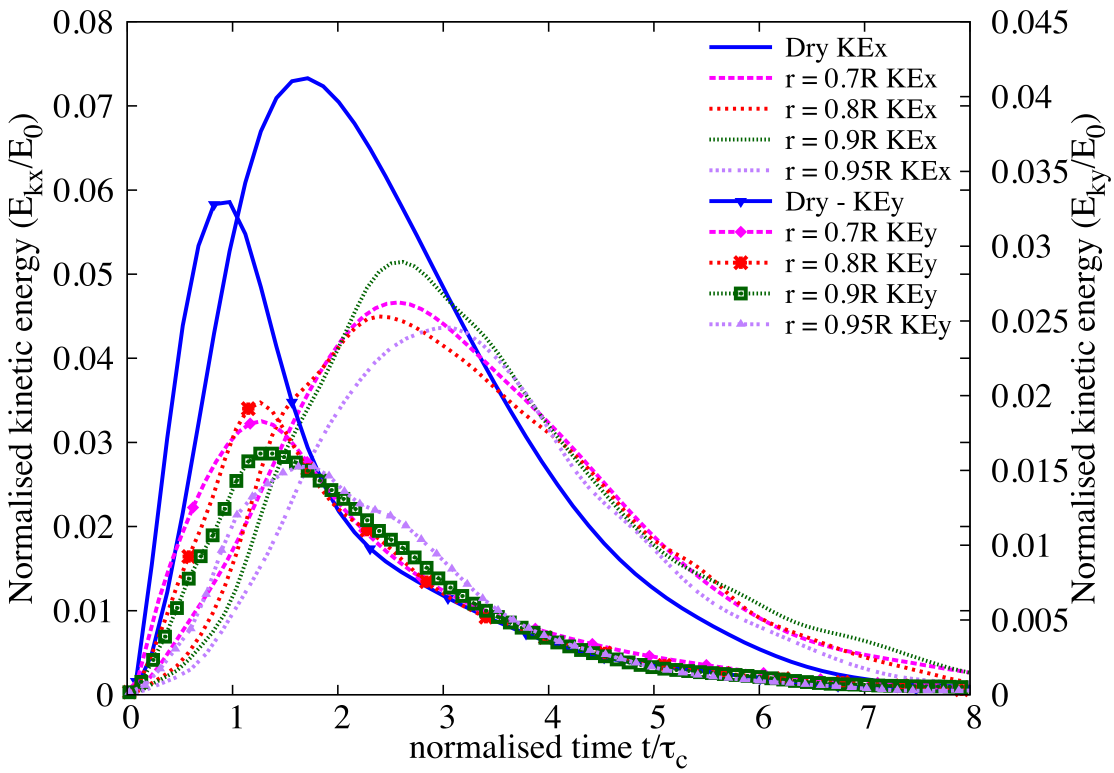

(b) Evolution of horizontal and vertical kinetic energies

Figure 6.29 Effect of permeability on the evolution of kinetic energies with time for a granular column collapse in fluid (a = 0.8 & loose packing)

Froude's number and the occurrence of hydroplaning in low permeability condition. Due to high permeability, the water entrained at the flow front is dissipated quicker and thus no lubrication effect is observed. A Froude's number of 0.272 (no hydroplaning) is observed for high permeability condition (r = 0.7 R). This shows that the drag force predominates at high permeability, while the low permeability condition is characterised by hydroplaning and lubrication.

Figure 6.31 shows the normalised pressure at the base for low and high permeability flows at $t = 2\tau_c$. The normalised effective stress plotted is obtained as the average over 5 time steps at $2\tau_c$. The effective stress at the base is normalised to the effective stress of a static granular column before collapse. A value of 1 indicates that the effective stress hasn't changed, which is observed in the static region of the granular column. It can be observed that the normalised effective stress is significantly high for low permeability condition at the flow front in comparison to almost non-existence of effective stress in low permeability condition. The observation of trivial effective stress at the flow front corroborates the lubrication effect observed at low permeability conditions.

Figure 6.32 shows the grain trajectories of a dense and a loose initial packing for a hydrodynamic radius (r = 0.95R). It can be observed that the dense initial packing results in a lot of turbulent behaviour at the flow surface in contrast to the more plug like flow observed in the loose condition. The thickness of the deposit in both dense and loose condition is almost the same, however the density of the flow results in a Froude's number of 0.46 and 0.429 for loose and dense conditions, respectively. The low initial density results in more hydroplaning in the loose condition. The effect of water entrainment at the flow front between dense and loose condition can be seen in figure 6.33. Comparing the packing density (see figures 6.20 and 6.28) reveals almost the same amount of water entrainment in both dense and loose conditions. Hence, it is the density of the flowing granular mass that controls the influence of hydroplaning for a given hydrodynamic radius and initial aspect ratio. A loosely packed granular column with low permeability entrains more water at the flow front, resulting in a hydroplaning effect that overcomes the influence of viscous drag forces and thereby yields a higher run-out distance than the dry condition.

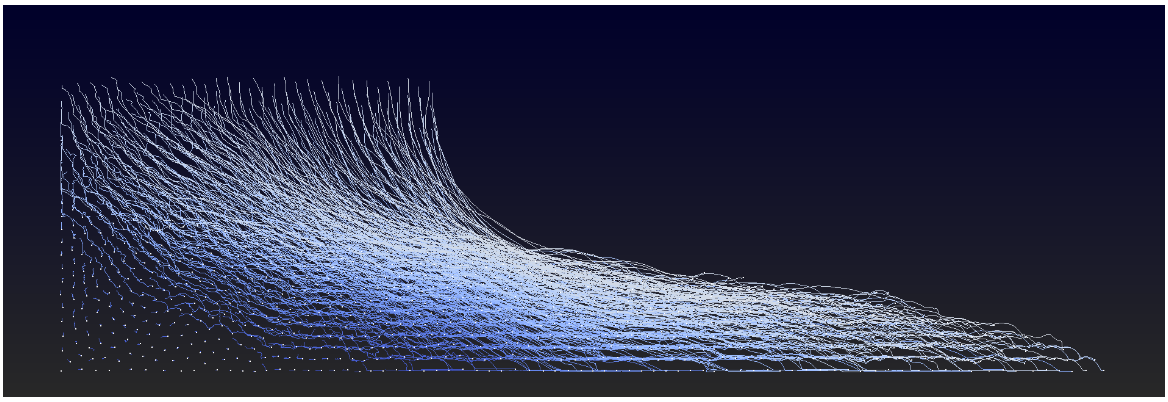

(a) High permeability (r = 0.7 R)

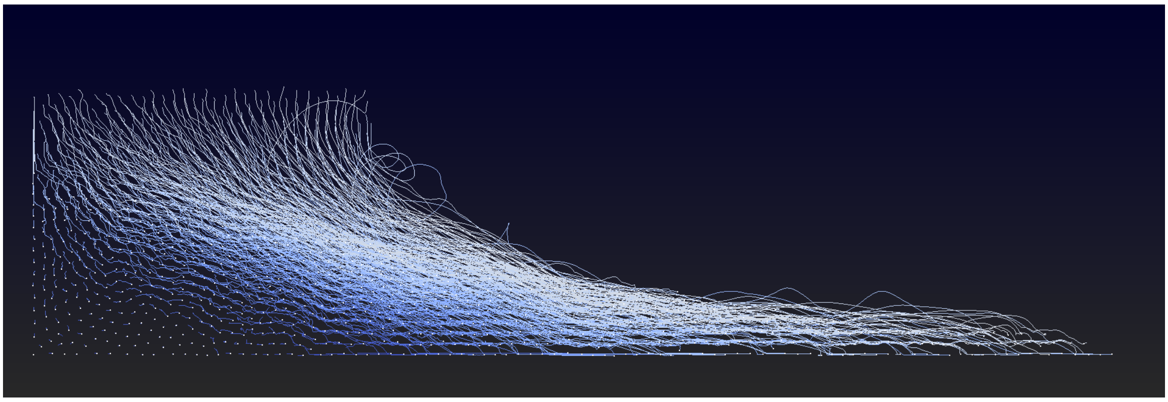

(b) Low permeability (r = 0.95 R)

Figure 6.30 Particle tracking of the deposit morphology for a granular column collapse in fluid (a = 0.8 & loose packing), influence of permeability

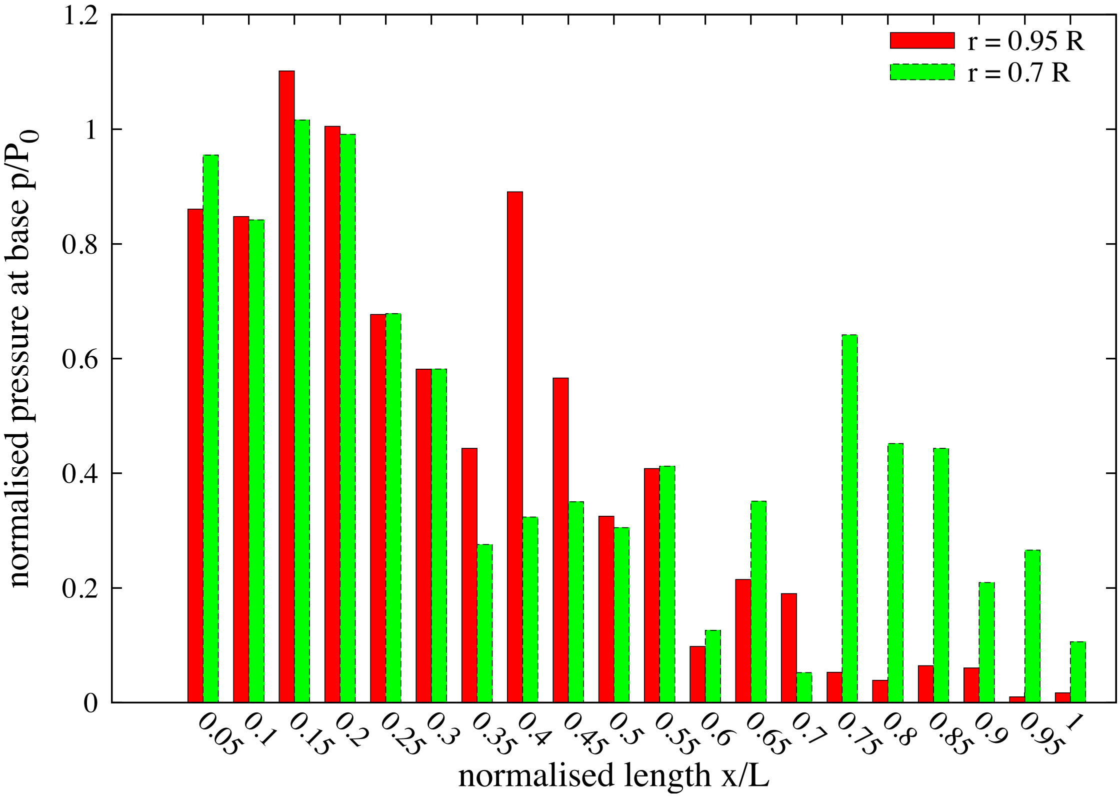

Figure 6.31 Effect of permeability on the normalised effective stress for loose initial packing at $t = 2\tau_c$

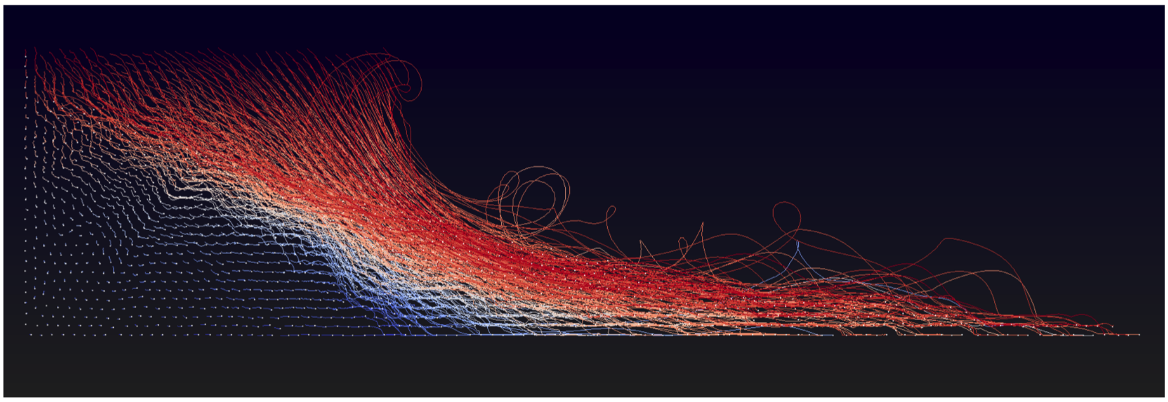

(a) Dense initial packing (83%)

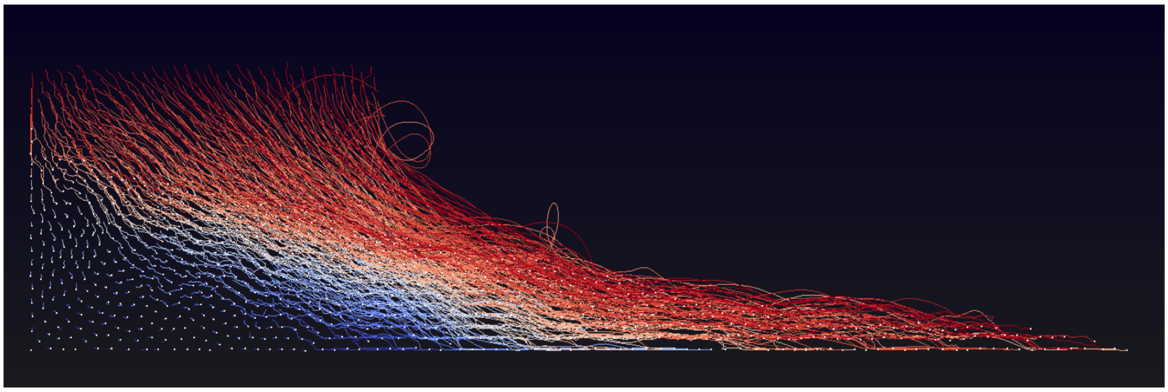

(b) Loose initial packing (79%)

Figure 6.32 Effect of initial density on the deposit morphology for a granular column collapse in fluid (a = 0.8). Dense vs loose initial packing fraction (r = 0.95R). Darker means dense packing, white indicates loose packing density.

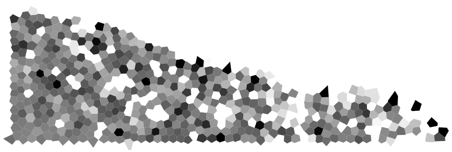

(a) Dense initial packing (83%)

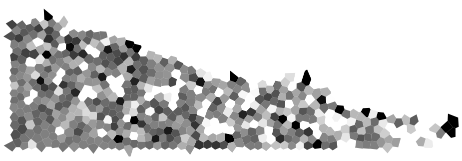

(b) Loose initial packing (79%)

Figure 6.33 Evolution of packing fraction at $t = \tau_c$ for dense and loose initial packing fraction.

6.4 Submarine granular flows down incline plane

Slope failure is a problem of high practical importance for both civil engineering structures and natural hazards management. Catastrophic events as landslides, debris flows, rock avalanches or reservoir embankment failures exemplify the potential consequences of a soil gravitational instability. One of the most critical situation concerns a submerged sandy slope since pore pressure changes, related to groundwater seepage flow or soil dilation/contraction, can significantly affect the stability of many earth structures or natural soils.

In this study, a 2D poly-disperse system ($d_{max}/d_{min} = 1.8$) of circular discs in fluid was used to understand the behaviour of granular flows on inclined planes (see **??**). The soil column was modelled using 1000 discs of density 2650 kg m^{-3} and a contact friction angle of 26°. The collapse of the column was simulated inside a fluid with a density of 1000 kg m^{-3} and a kinematic viscosity of 1×10^{-6} m^2 s^{-1}. The choice of a 2D geometry has the advantage of cheaper computational effort than a 3D case, making it feasible to simulate very large systems. A granular column of aspect ratio 'a' of 0.8 was used. A hydrodynamic radius r = 0.9R was adopted during the LBM computations. Dry analyses were also performed to study the effect of hydrodynamic forces on the run-out distance.

6.4.1 Effect of initial density

The morphology of the granular deposits in fluid is shown to be mainly controlled by the initial volume fraction of the granular mass and not by the aspect ratio of the column (Pailha et al., 2008; Rondon et al., 2011). In order to understand the influence of the initial packing density on the run-out behaviour, a dense sand column (initial packing density, $\Phi = 83\%$) and a loose sand column ($\Phi = 79\%$) were used. The granular columns collapse and flow down slopes of varying inclinations (2.5°, 5° and 7.5°).

The evolution of run-out distances for a dense sand column with time in dry and submerged conditions for varying slope inclinations are presented in figure 6.34. The run-out distance is longer in submerged condition than the dry condition for a flow on a horizontal surface. However, with increase in the slope angle the run-out in the fluid decreases.

Dense granular columns in fluid take a longer time to collapse and flow, due to the development of large negative pore-pressures, as the dense granular material dilates during the initial phase of the flow. The morphology of dense granular flows down slopes of varying inclinations at the critical time ($t = \tau_c = \sqrt{H/g}$, when the flow is fully mobilised) are shown in figure 6.36.

It can be seen that the viscous drag on the dense column tend to predominate over the influence of hydroplaning on the run-out behaviour. This influence can be observed in the smaller peak kinetic energy for granular column in fluid compared to it's dry counterpart

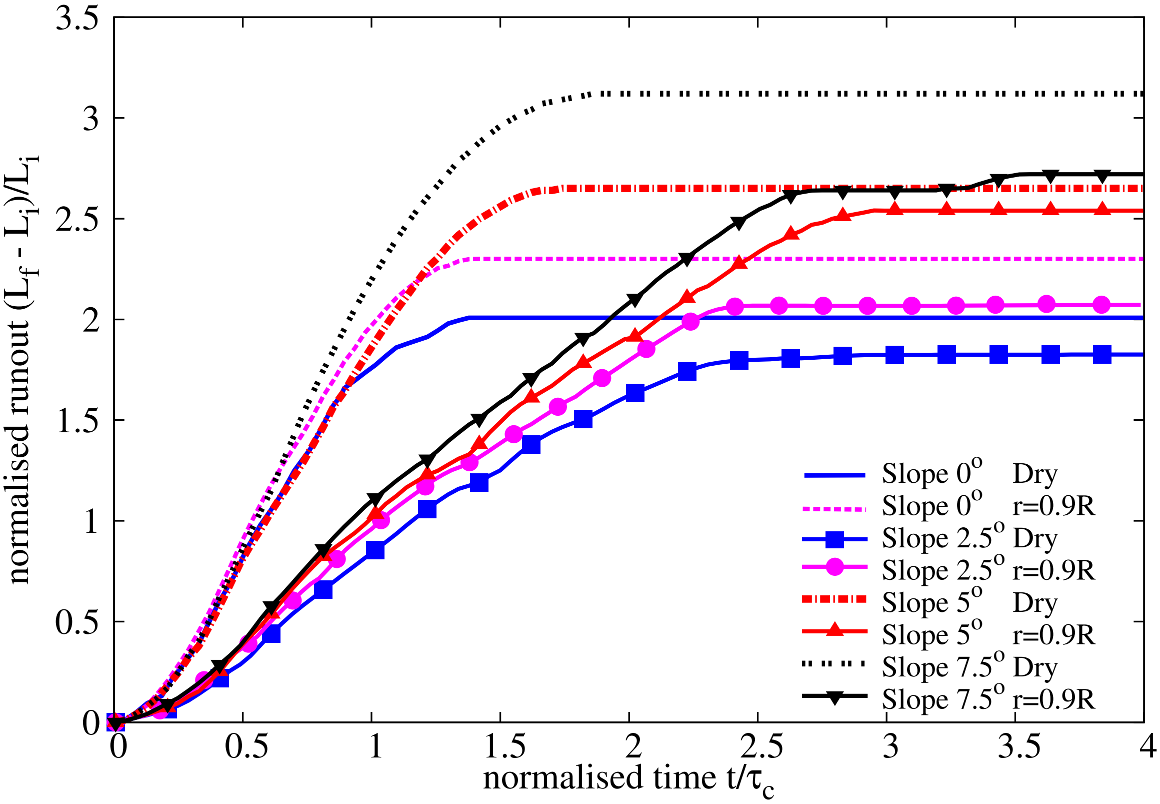

Figure 6.34 Evolution of run-out with time (dense)

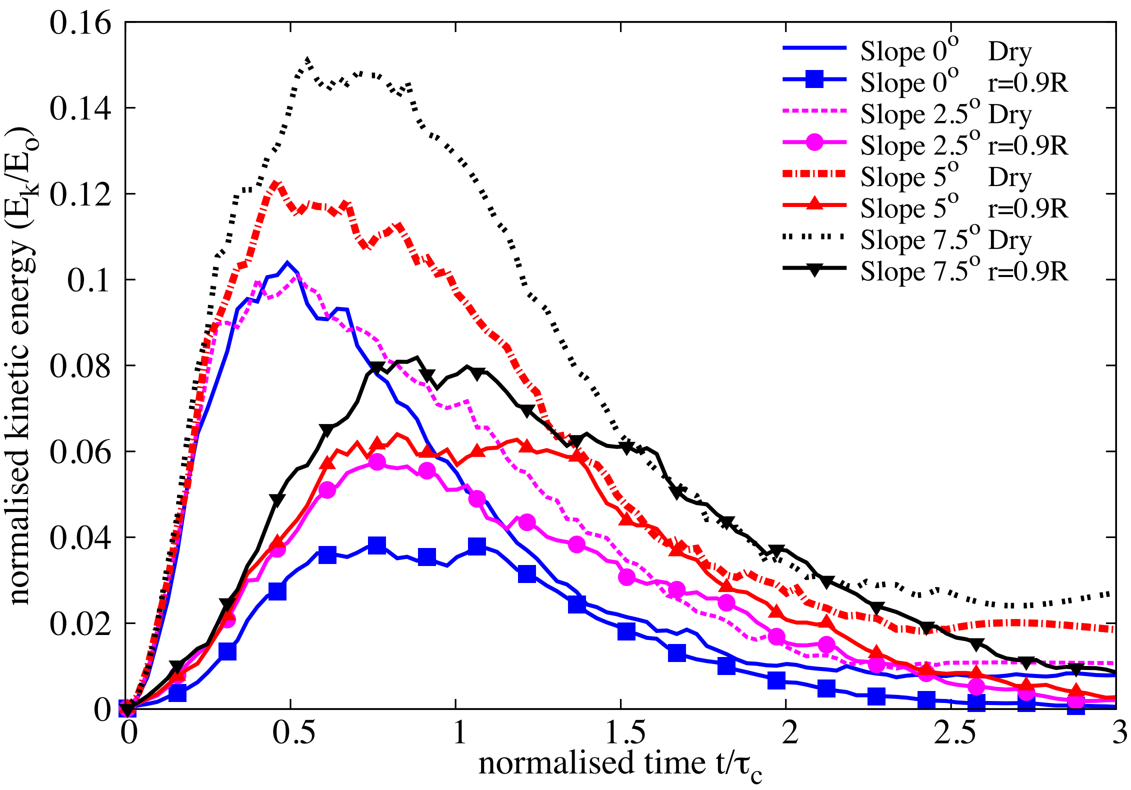

Figure 6.35 Evolution of Kinetic Energy with time (dense case)

(see Figure 6.35). With increase in slope angle, the volume of material that dilates increases. This results in large negative pore pressures and more viscous drag on the granular material. Hence, the difference in the run-out between the dry and the submerged condition, for a dense granular assembly, increases with increase in the slope angle.

In contrast to the dense granular columns, the loose granular columns (relative density $I_D = 30\%$) show longer run-out distance in immersed conditions (see Figure 6.37). The run-out distance in fluid increases with increase in the slope angle compared to the dry cases. Loose granular material tends to entrain more water at the base of the flow front, creating a lubricating surface, which causes longer run-out distance (see Figure 6.38). The hydroplaning effect causes an increase in the velocity the loose condition in comparison with the dense condition (see Figure 6.39).

The evolution of packing density (see Figure 6.40) shows that dense and the loose conditions reach similar packing density. This indicates that the dense granular column dilates more and is susceptible to higher viscous drag forces. Where as in the loose condition, a positive pore-pressure is observed at the base of the flow, indicating entrainment of water at the base, i.e. hydroplaning resulting in longer run-out distance.

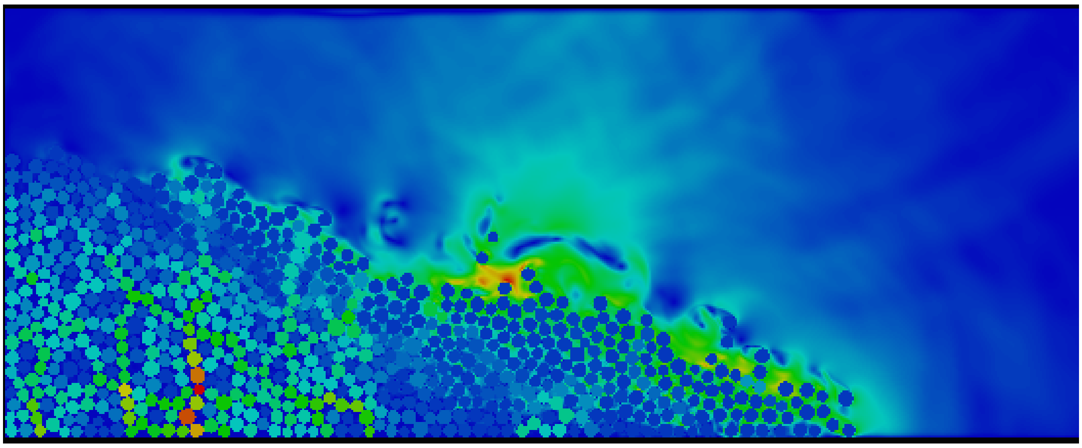

(a) Slope 2.5

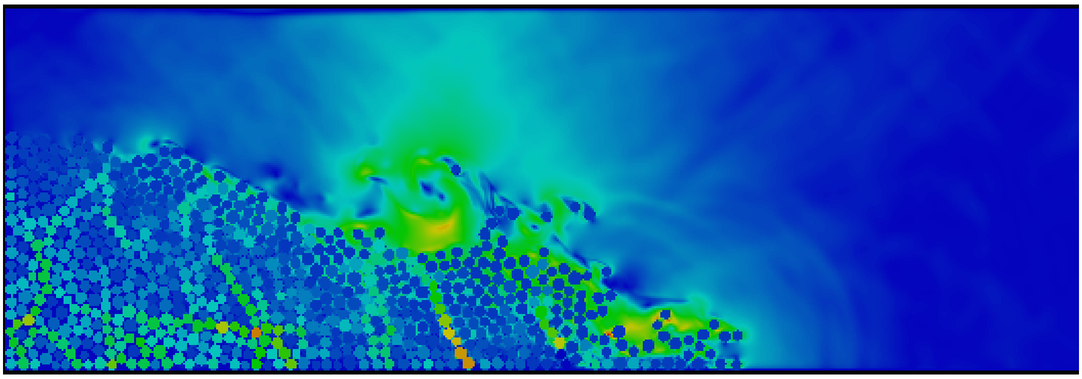

(b) Slope 5.0

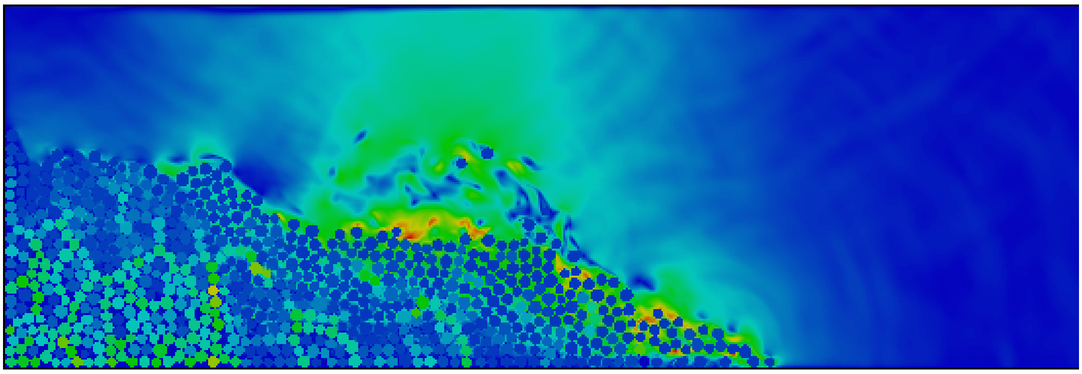

(c) Slope 7.5

Figure 6.36 Flow morphology at critical time for different slope angles (dense)

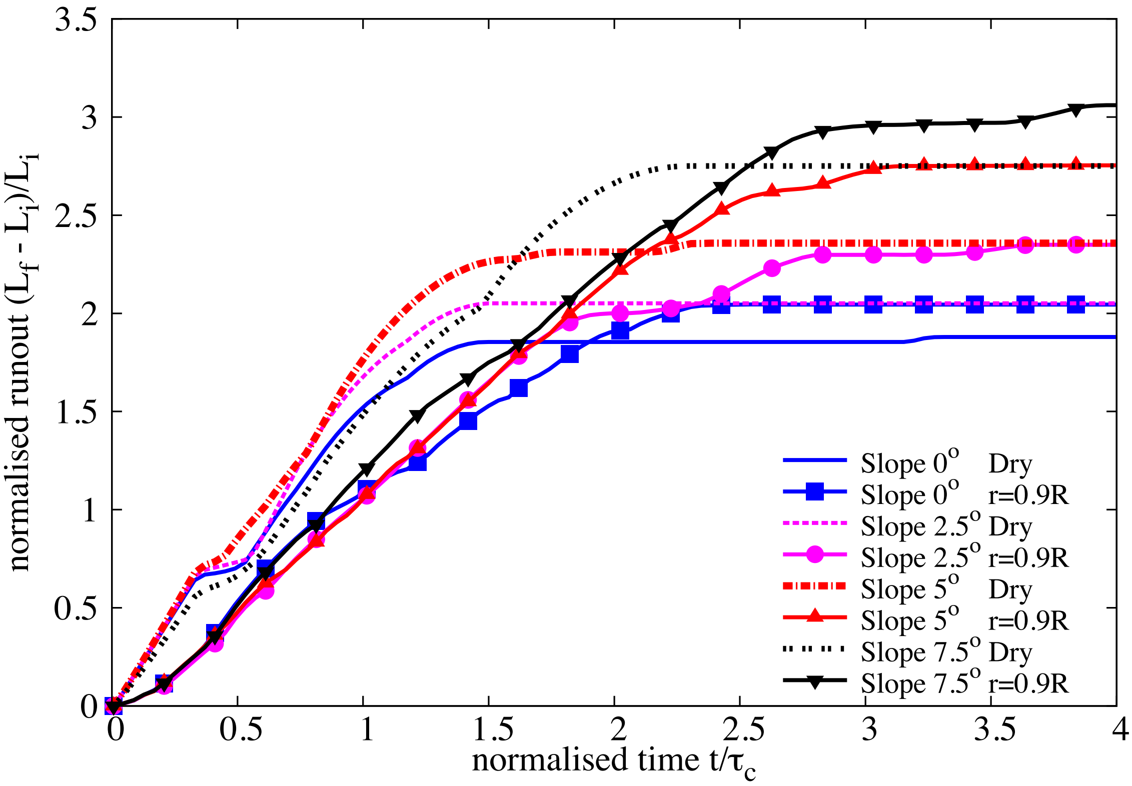

Figure 6.37 Evolution of run-out with time (loose)

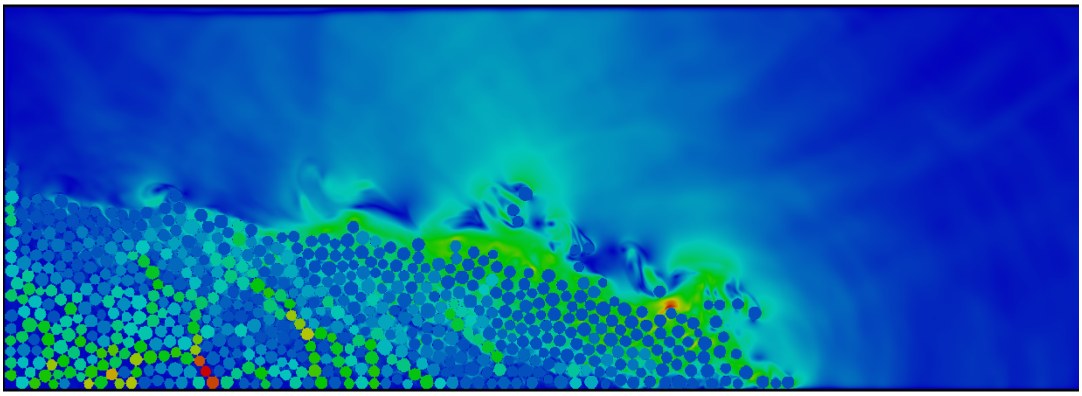

(a) Slope 2.5

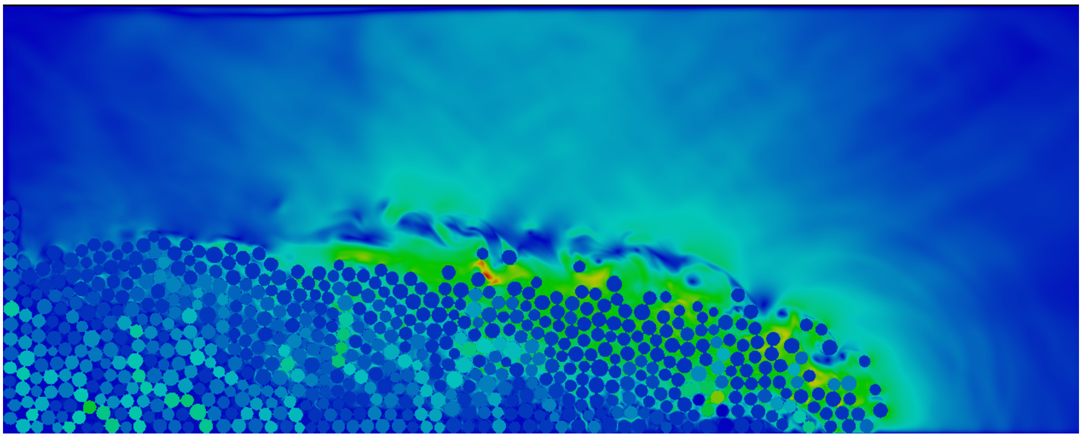

(b) Slope 5.0

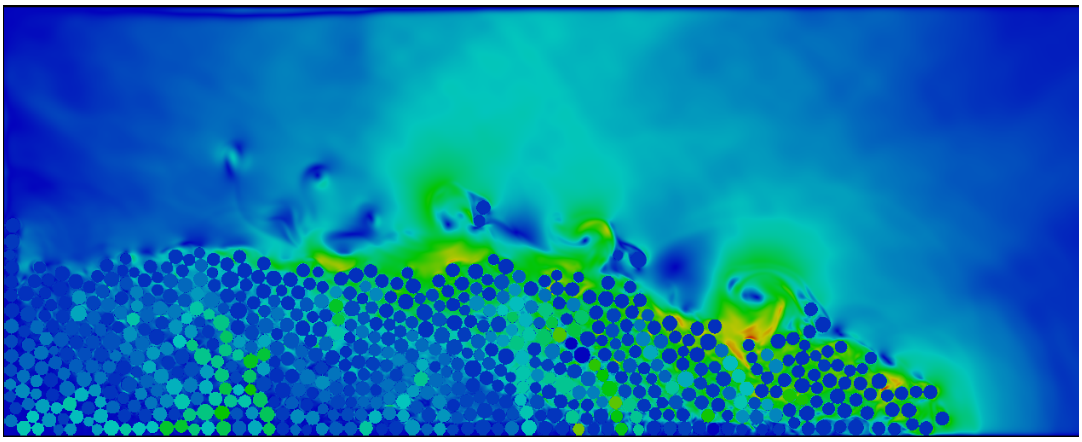

(c) Slope 7.5

Figure 6.38 Flow morphology at critical time for different slope angles (loose)

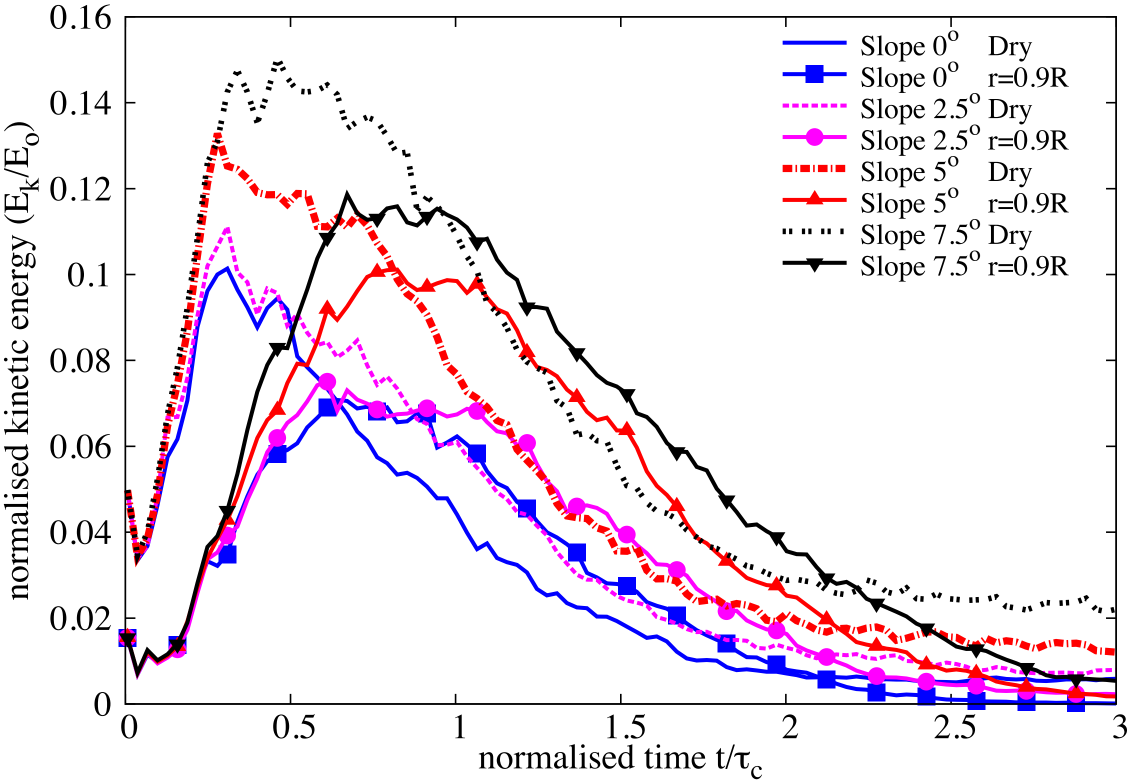

Figure 6.39 Evolution of Kinetic Energy with time (loose)

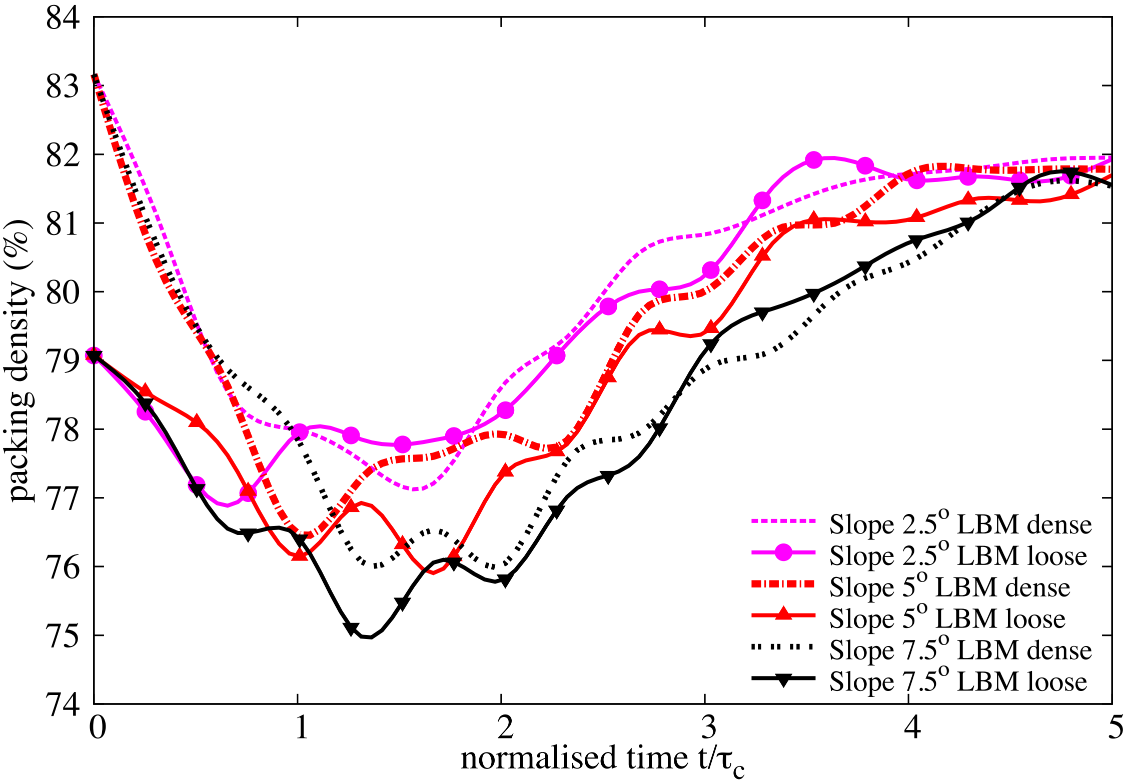

Figure 6.40 Evolution of packing density with time

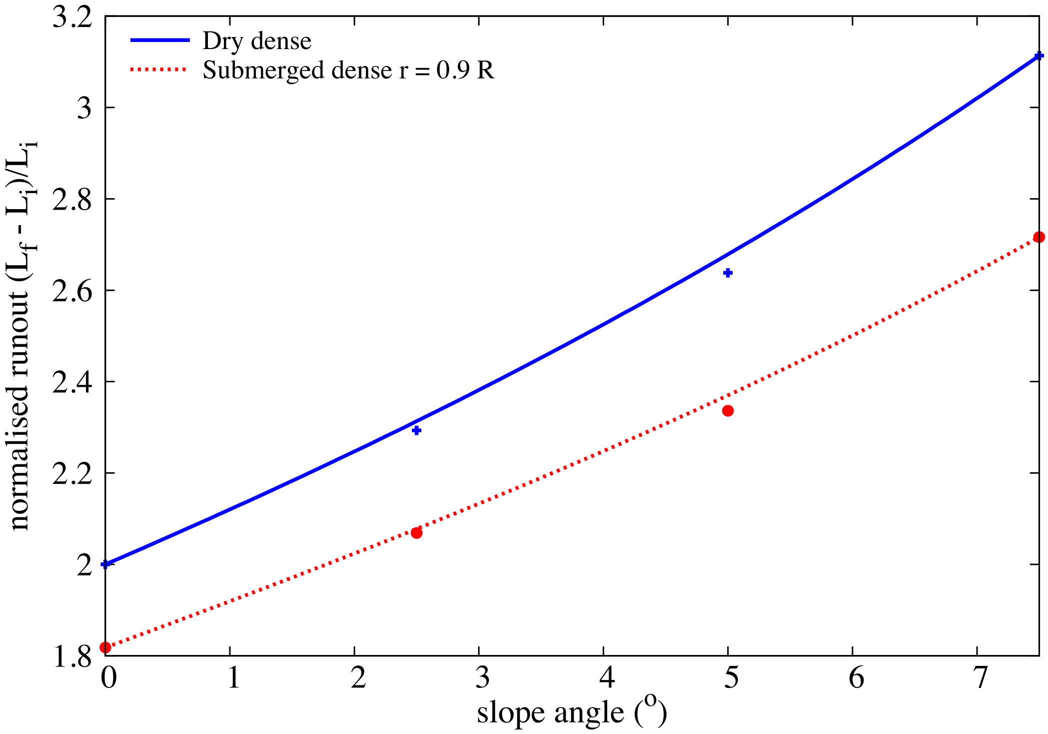

(a) Effect of slope angle on the run-out distance (Dense). Comparison between dry and submerged granular column.

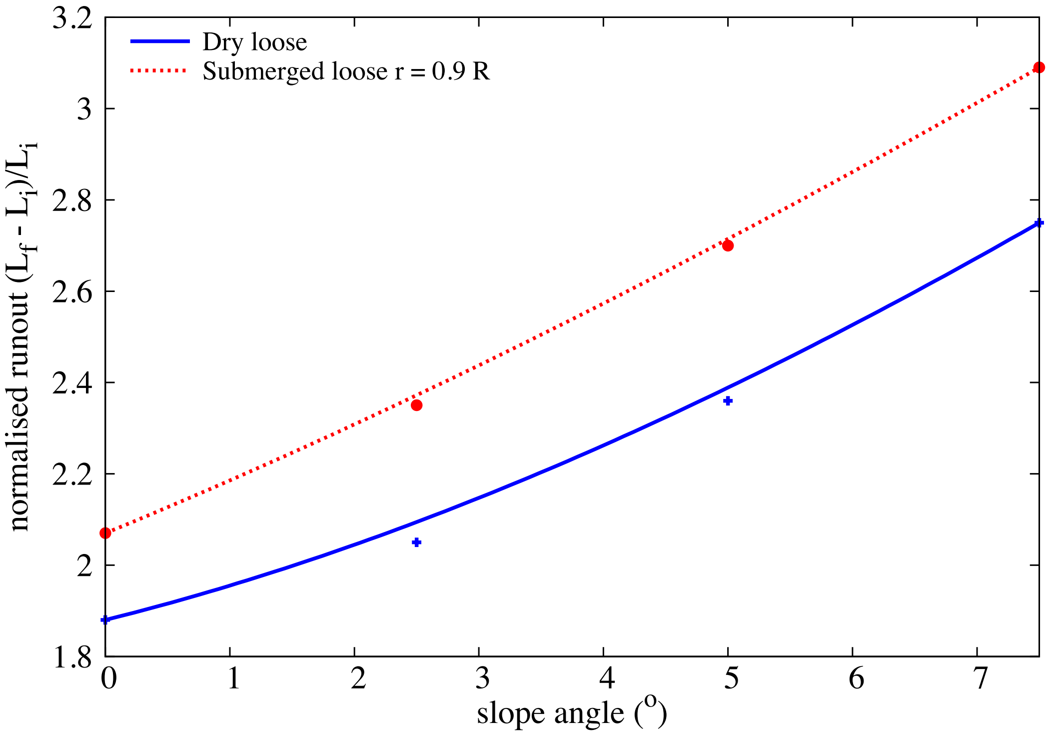

(b) Effect of slope angle on the run-out distance (Loose). Comparison between dry and submerged granular column.

Figure 6.41 Effect of slope angle on the run-out distance (Dense and Loose). Comparison between dry and submerged granular column.

6.4.2 Effect of permeability

For a slope angle of 5°, the hydrodynamic radius of the loosely packed grains was varied from r = 0.7R (high permeability), 0.75R, 0.8R, 0.85R to 0.9R (low permeability). The run-out distance is found to increase with decrease in the permeability of the granular assembly (see Figure 6.42). The run-out distance for high permeable conditions (r = 0.7R – 0.8R) were lower than their dry counterparts. Although, decrease in permeability resulted in an increase in the run-out distance, no significant change in the run-out behaviour was observed for a hydrodynamic radius of up to 0.8R.

With further decrease in permeability (r = 0.85R and 0.9R), the run-out distance in the fluid was greater than the run-out observed in the dry condition. At very low permeability (r = 0.9R), granular material started to entrain more water at the base, which causes a reduction in the effective stress accompanied by a lubrication effect on the flowing granular media. This can be seen as a significant increase in the peak kinetic energy and the duration of the peak energy, in comparison with dry and high permeable conditions (see Figure 6.44).

The permeability of the granular column did not have an influence on the evolution of height during the flow. However, dry granular column tends to collapse more than the immersed granular column (see Figure 6.43).

Positive pore-pressure generation at the base of the flow was observed for low permeable conditions. Inspection of the local packing density showed entrainment of water at the base of the flow, which can also be observed by the steep decrease in the packing density (see Figure 6.45) for the very low permeability condition (r = 0.9R). At the end of the flow ($t \geq 3 \times \tau_c$), the excess pore-pressure dissipates and the granular material, irrespective of their permeability, reaches almost the same packing density.

6.5 Tall columns

6.6 Summary

Two-dimensional LB-DEM simulations were performed to understand the behaviour of submarine granular flows. Unlike dry granular collapse, the run-out behaviour in fluid is dictated by the initial volume fraction. Granular columns with loose packing tend to flow longer in comparison to dense columns, due to entrainment of water at the base resulting in lubrication. The loose column when it starts flowing expands and ejects liquid, leading to a partial fluidization of the material. However, with increase in the slope angle, the run-out in fluid is influenced by the viscous drag on the granular materials. The run-out distance in fluid increases with decrease

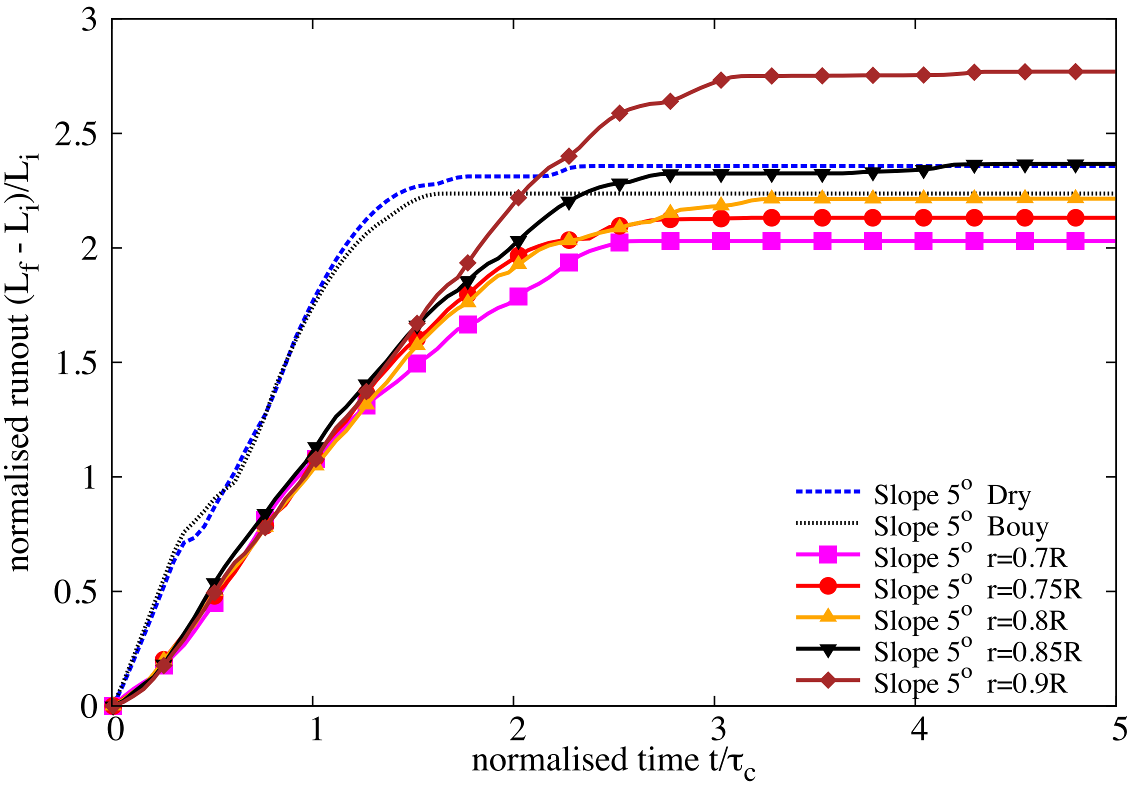

Figure 6.42 Evolution of run-out with time for different permeability (loose slope 5°)

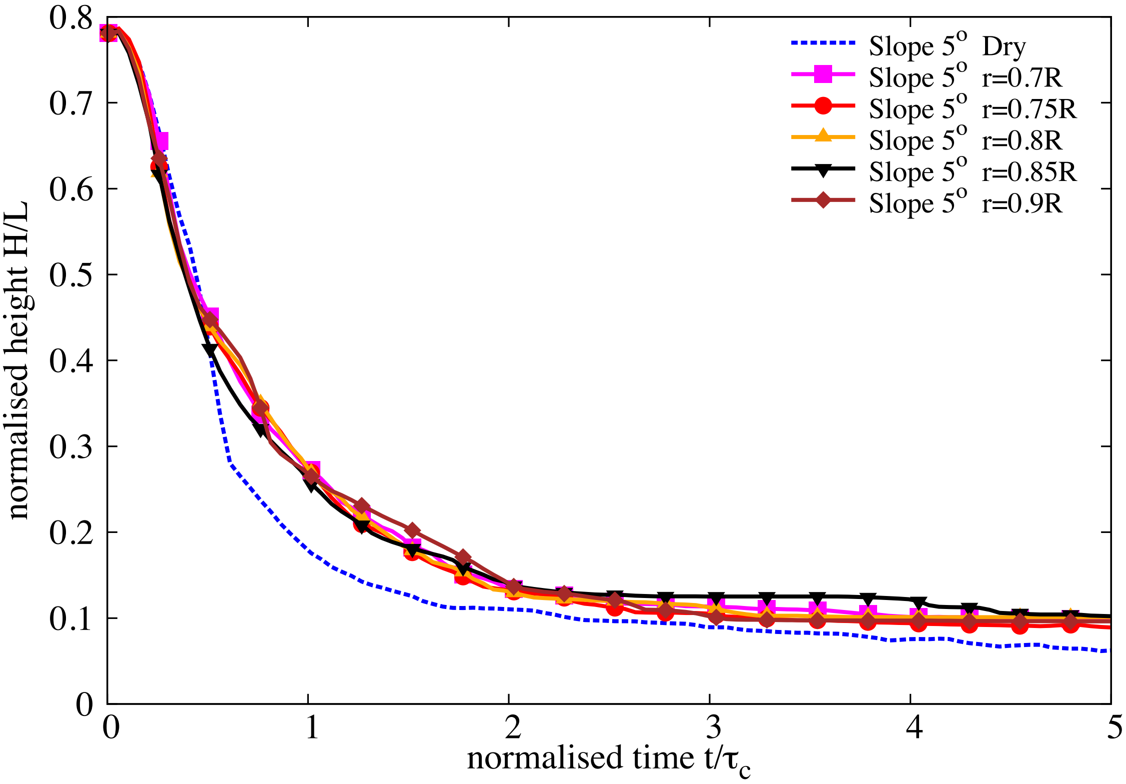

Figure 6.43 Evolution of height with time for different permeability (loose slope 5°)

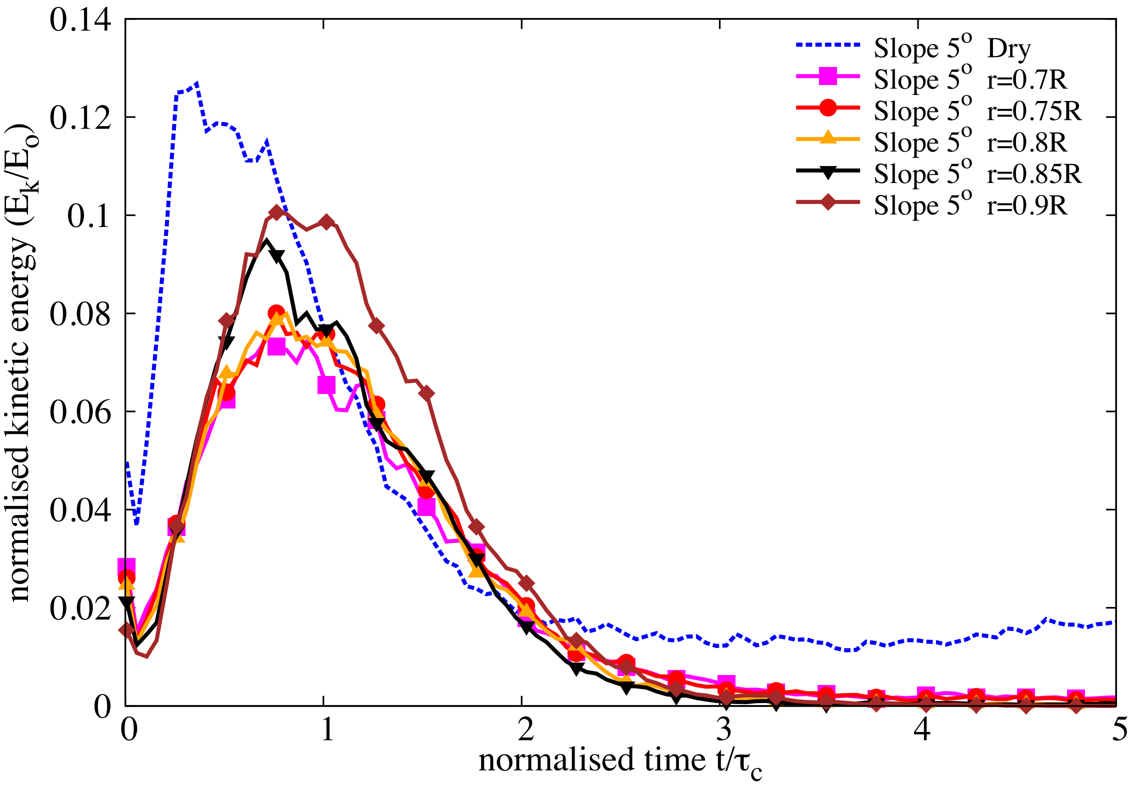

Figure 6.44 Evolution of Kinetic Energy with time for different permeability (loose slope 5°)

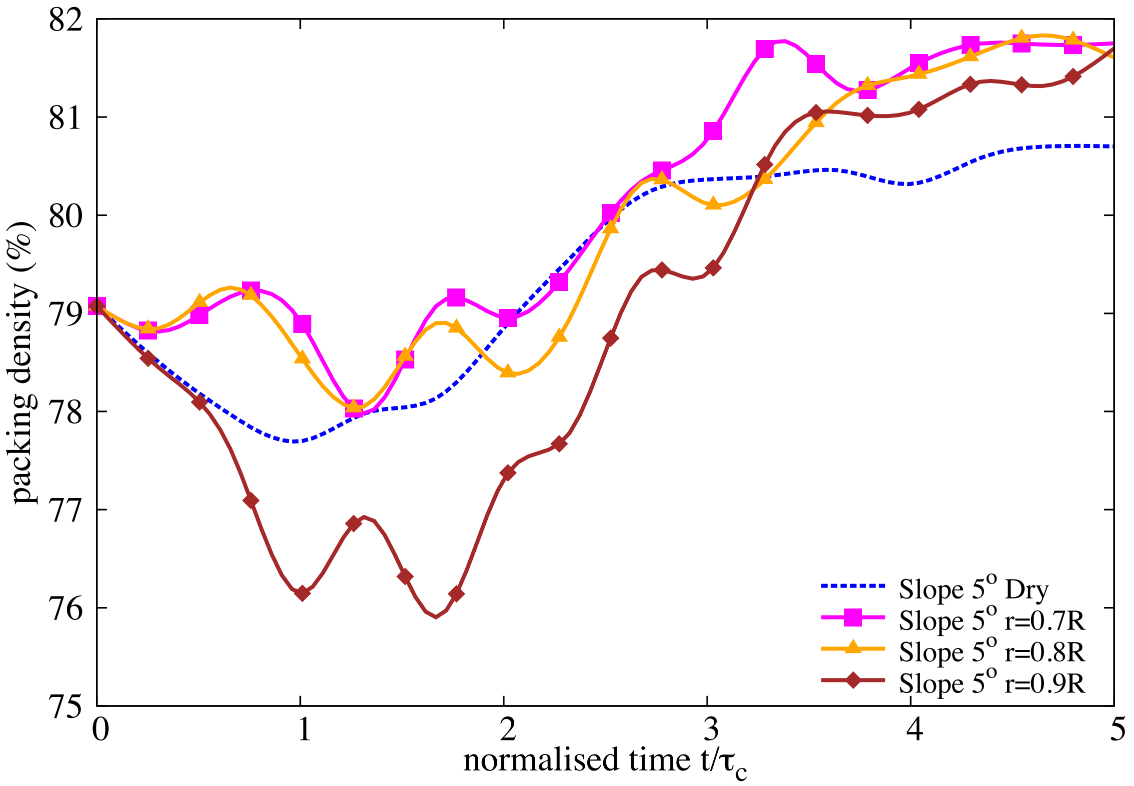

Figure 6.45 Evolution of packing density with time for different permeability (loose slope 5°)

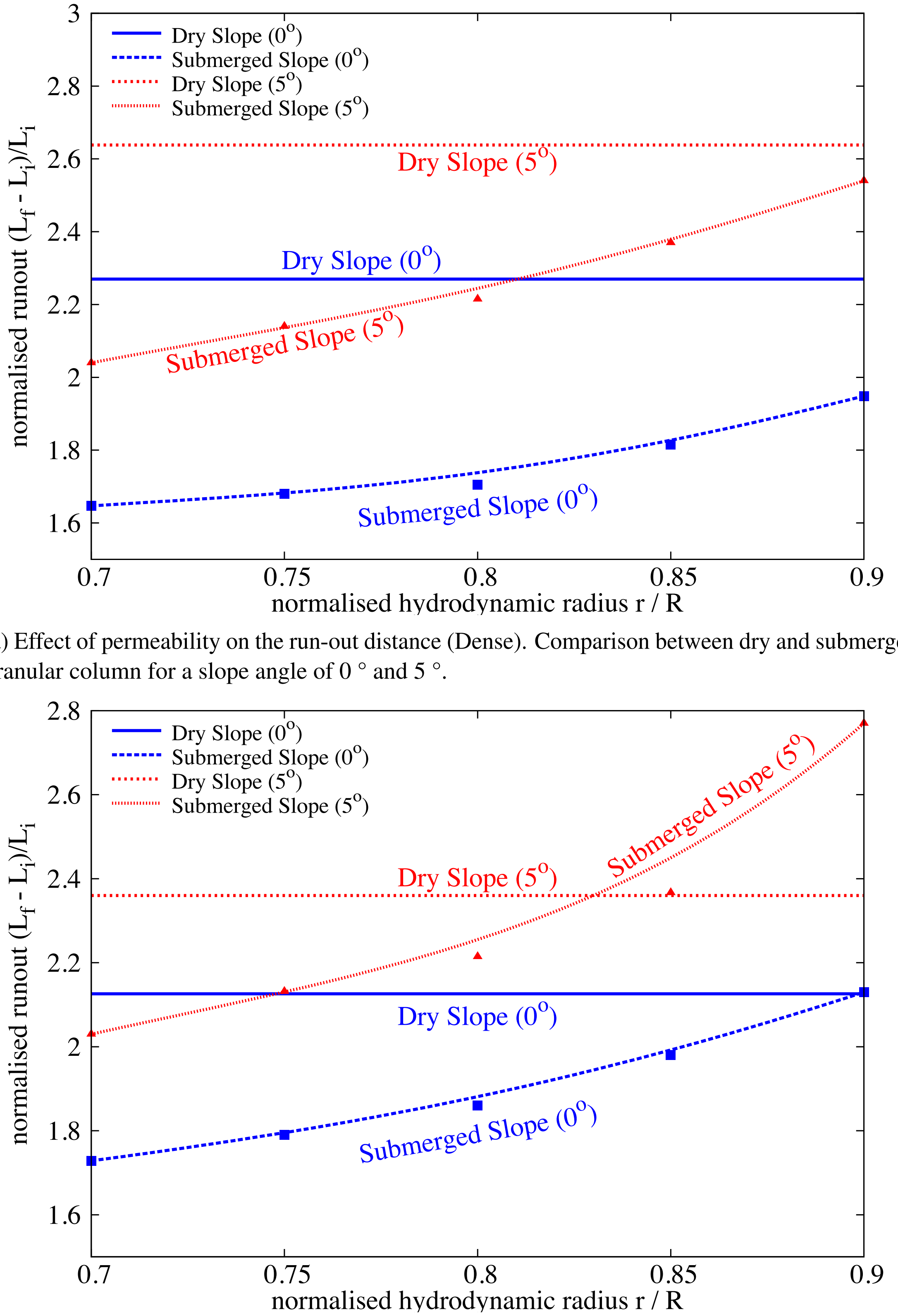

(a) Effect of permeability on the run-out distance (Dense). Comparison between dry and submerged granular column for a slope angle of 0 ° and 5 °.

(b) Effect of permeability on the run-out distance (Loose). Comparison between dry and submerged granular column for a slope angle of 0 ° and 5 °.

Figure 6.46 EEffect of permeability on the run-out distance (Dense and Loose). Comparison between dry and submerged granular column for a slope angle of 0 ° and 5 °..

(a) t=0

(b) t=τ_c

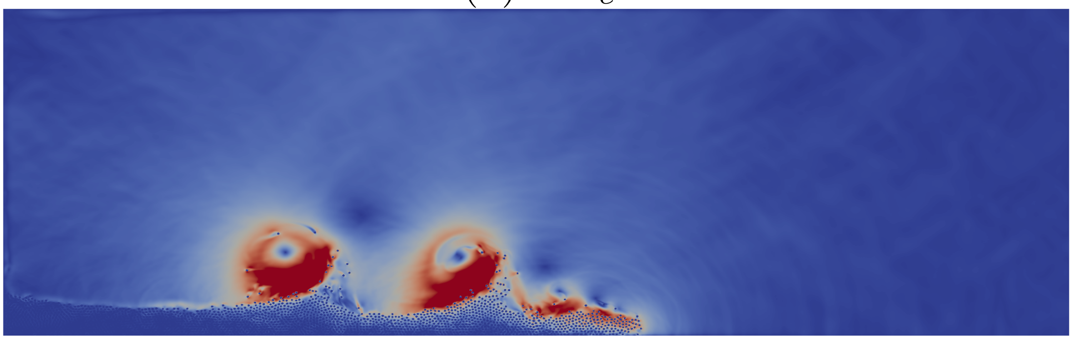

(c) t=$3 \times \tau_c$

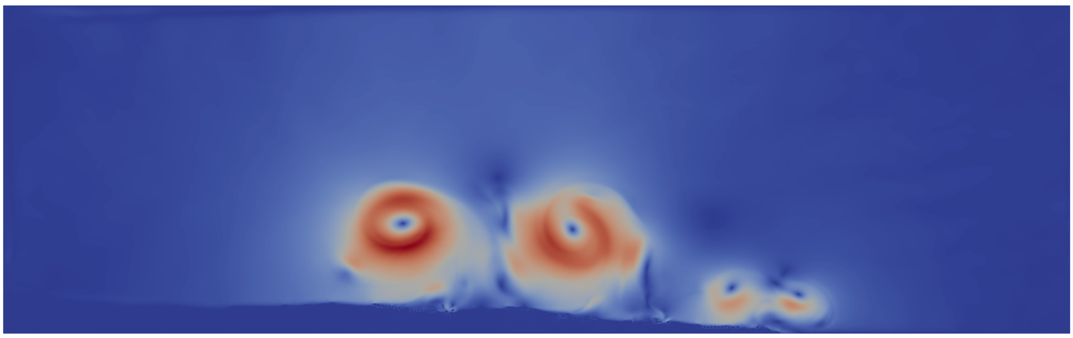

(d) t=$6 \times \tau_c$

Figure 6.47 Flow evolution of a granular column collapse in fluid (a = 6) on a horizontal surface

$t = 0\tau_c$

$t = 1\tau_c$

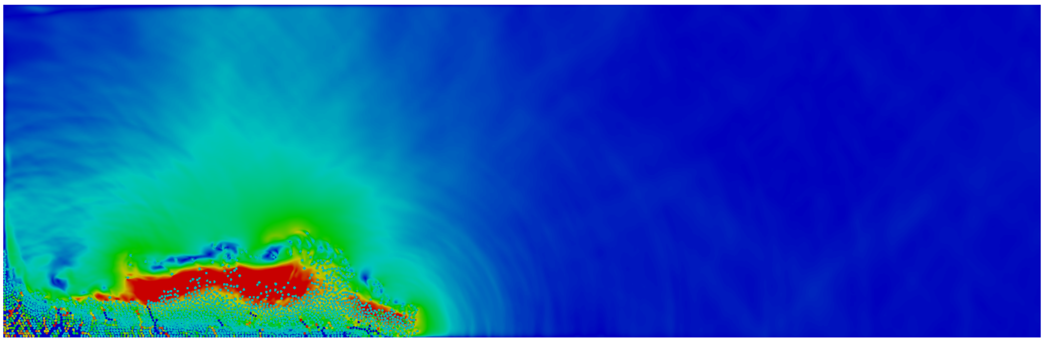

$t = 3\tau_c$

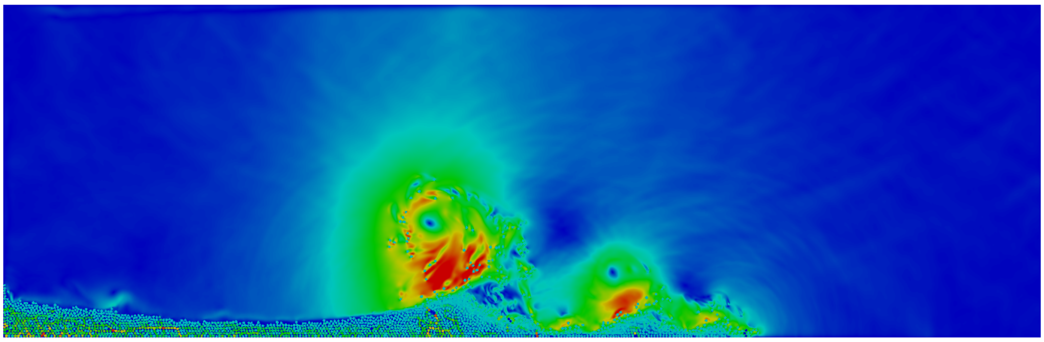

$t = 6\tau_c$

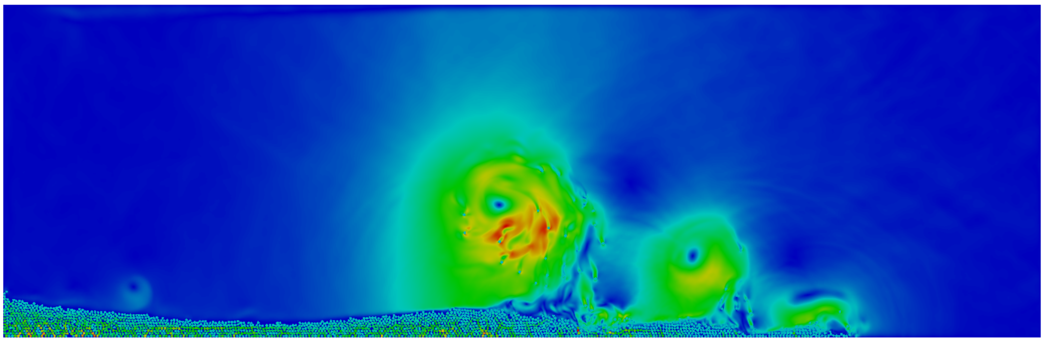

$t = 8\tau_c$

Figure 6.47 Flow evolution of a granular column collapse in fluid (a = 6) on a slope of 5°. Shows the velocity profile of fluid due to interaction with the grains (red - higher velocity).

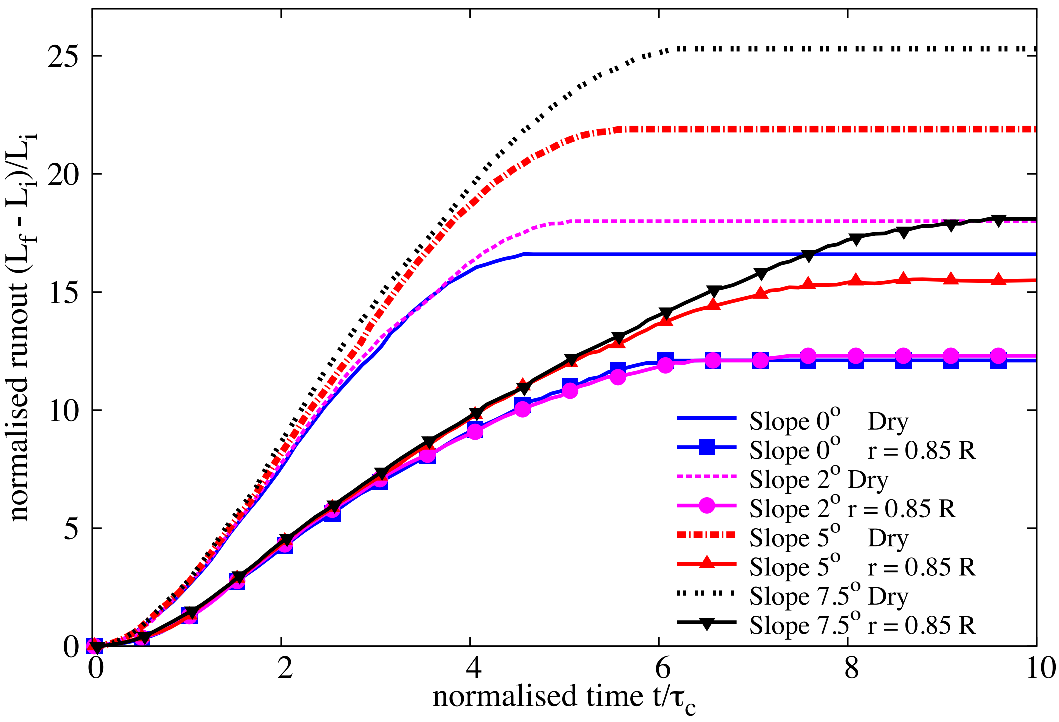

Figure 6.48 Evolution of run-out for a column collapse in fluid (a = 6) on a slope of 5°

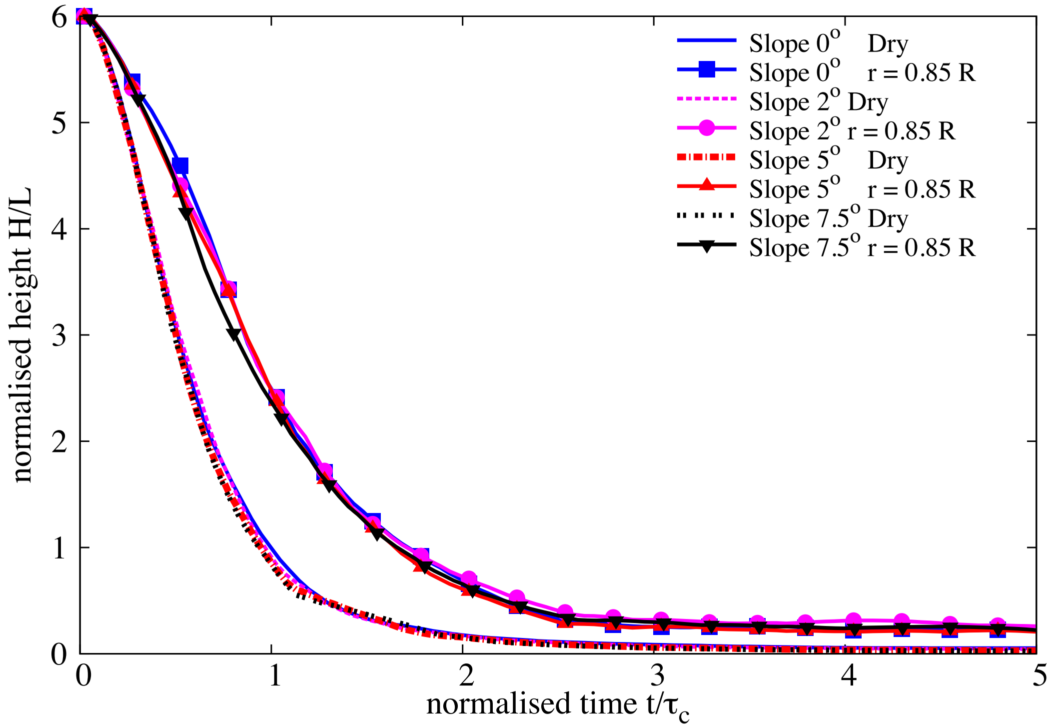

Figure 6.49 Evolution of height with time for a column collapse in fluid (a = 6) on a slope of 5°

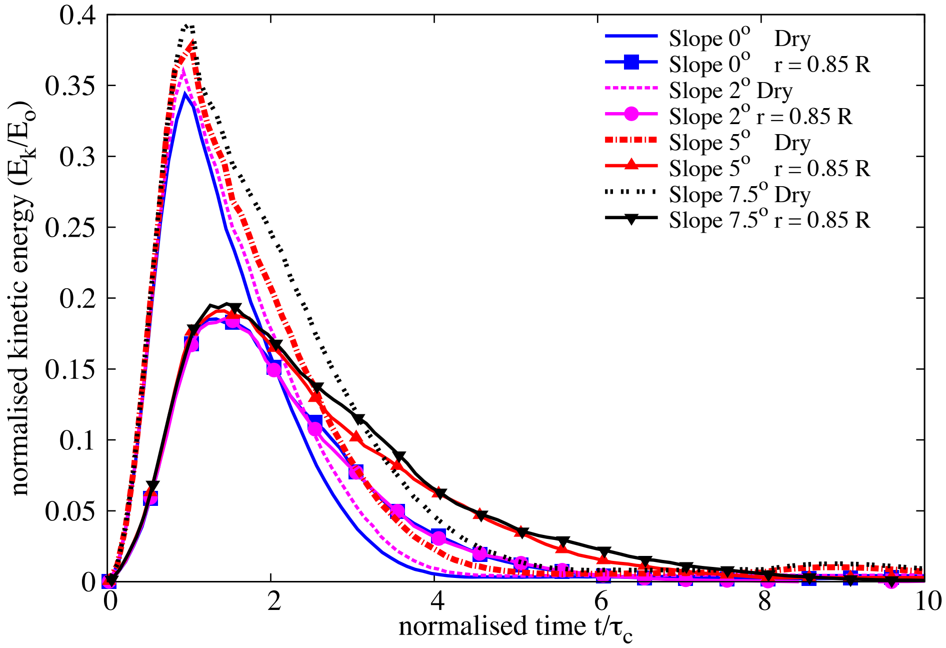

(a) Evolution of the total kinetic energy

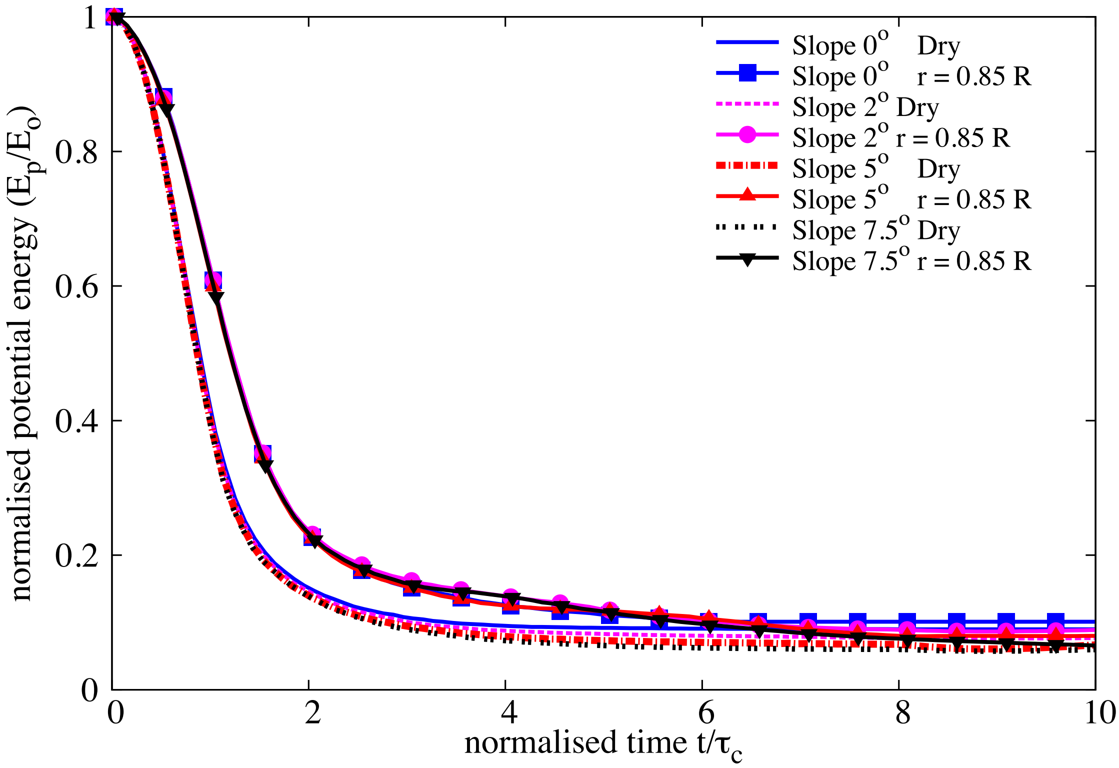

(b) Evolution of the total potential energy

Figure 6.50 Evolution of the kinetic and the potential energy with time for a granular column collapse in fluid (a = 6) on a slope of 5°

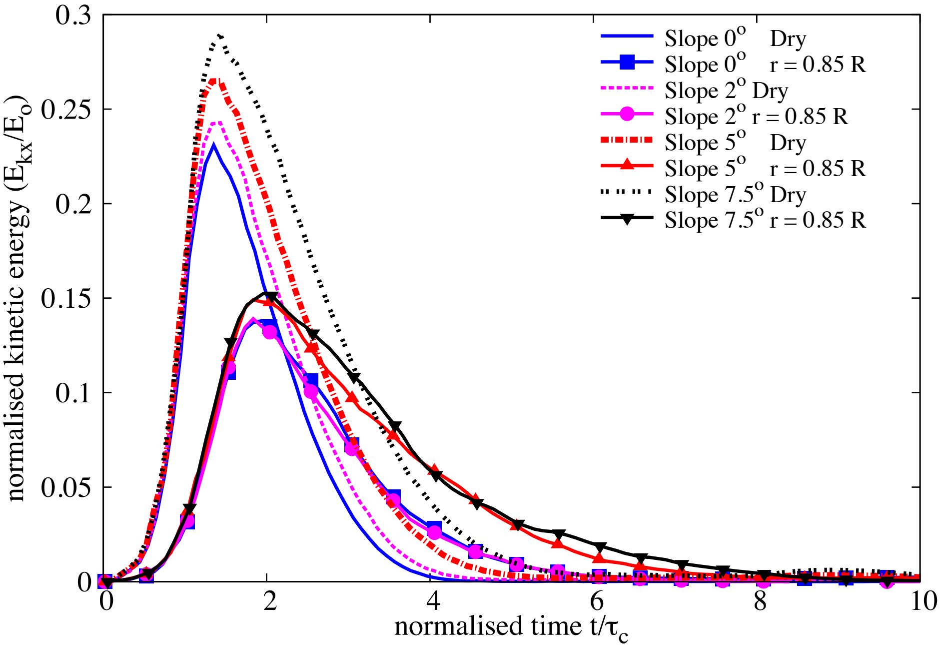

(a) Evolution of the vertical kinetic energy

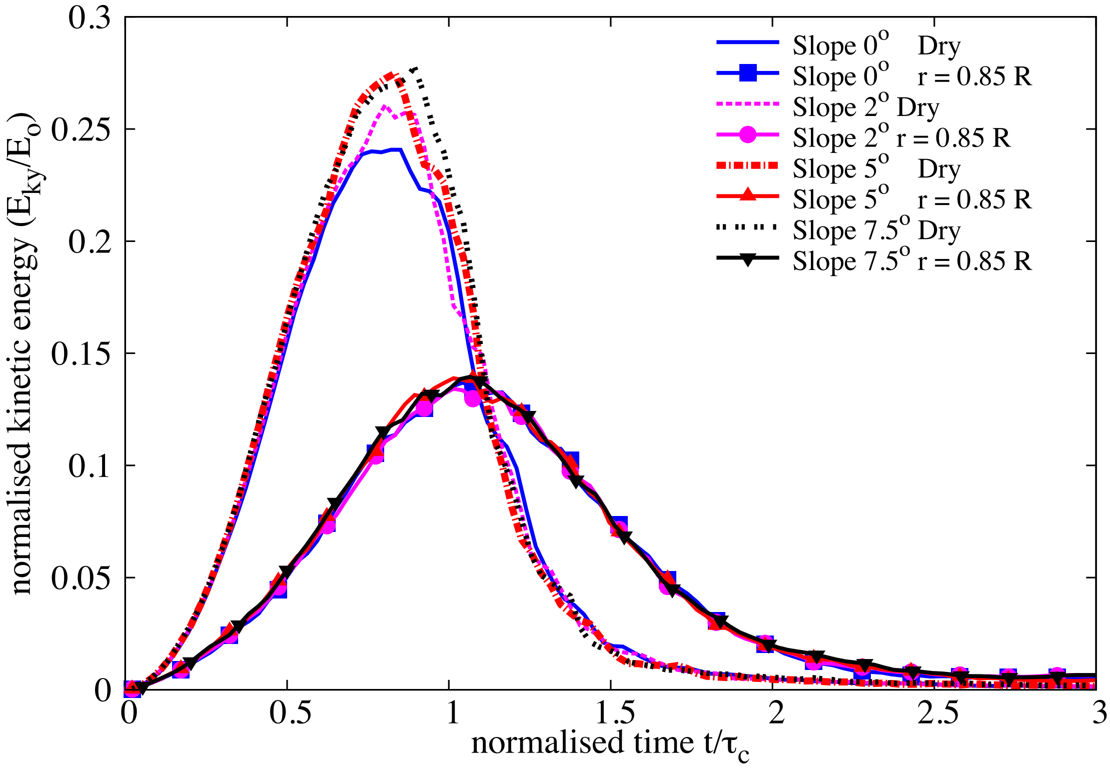

(b) Evolution of the horizontal kinetic energy

Figure 6.51 Evolution of the kinetic energies with time for a granular column collapse in fluid (a = 6) on a slope of 5°

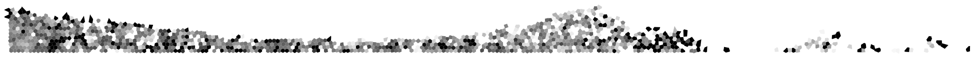

$t = 6\tau_c$

$t = 8\tau_c$

Figure 6.52 Packing density of a granular column collapse in fluid (a = 6) on a slope of 5°.

in permeability. More research work is required to characterise the flow behaviour of granular materials, especially in submerged conditions.

References

Bonnet, F., Richard, T., and Philippe, P. (2010). Sensitivity to solid volume fraction of gravitational instability in a granular medium. *Granular Matter*.

Denlinger, R. and Iverson, R. (2001). Flow of variably fluidized granular masses across three-dimensional terrain, ii: Numerical predictions and experimental tests. *J. Geophys. Res*, 106(B1):553–566.

Harbitz, C. B. (2003). Hydroplaning of subaqueous debris flows and glide blocks: Analytical solutions and discussion. *Journal of Geophysical Research*, 108(B7):2349.

Iverson, R. M. (2000). Acute Sensitivity of Landslide Rates to Initial Soil Porosity. *Science*, 290(5491):513–516.

Kumar, K., Soga, K., and Delenne, J.-Y. (2012). *Discrete Element Modelling of Particulate Media*. Special Publication. Royal Society of Chemistry, Cambridge.

Meruane, C., Tamburrino, A., and Roche, O. (2010). On the role of the ambient fluid on gravitational granular flow dynamics. *Journal of Fluid Mechanics*, 648:381–404.

Midi, G. D. R. (2004). On dense granular flows. *European Physical Journal E*, 14(4):341–365.

Mohrig, D. and Ellis, C. (1998). Hydroplaning of subaqueous debris flows. *...Society of America ...*.

Pailha, M., Pouliquen, O., and Nicolas, M. (2008). Initiation of Submarine Granular Avalanches: Role of the Initial Volume Fraction. *AIP Conference Proceedings*, 1027(1):935–937.

Peker, S. and Helvacı, S. (2007). *Solid-liquid two phase flow*. Elsevier.

Rondon, L., Pouliquen, O., and Aussillous, P. (2011). Granular collapse in a fluid: Role of the initial volume fraction. *Physics of Fluids*, 23(7):073301–073301–7.

Thompson, E. L. and Hupper, H. E. (2007). Granular column collapses: Further experimental results. *Journal of Fluid Mechanics*, 575:177–186.

Topin, V., Dubois, F., Monerie, Y., Perales, F., and Wachs, A. (2011). Micro-rheology of dense particulate flows: Application to immersed avalanches. *Journal of Non-Newtonian Fluid Mechanics*, 166(1-2):63–72.

Topin, V., Monerie, Y., Perales, F., and Radjaï, F. (2012). Collapse Dynamics and Runout of Dense Granular Materials in a Fluid. *Physical Review Letters*, 109(18):188001.

Yazdchi, K., Srivastava, S., and Luding, S. (2011). Microstructural effects on the permeability of periodic fibrous porous media. *International Journal of Multiphase Flow*.